

Histone proteomics reveals novel post-translational modifications in breast cancer

Angela Mena Perri^{1,*}, Valter Agosti^{2,*}, Erika Olivo¹, Antonio Concolino¹, MariaTeresa De Angelis³, Laura Tammè¹, Claudia Vincenza Fiumara¹, Giovanni Cuda^{1,#}, Domenica Scumaci^{1,#}

¹Laboratory of Proteomics, Research Center on Advanced Biochemistry and Molecular Biology, Department of Experimental and Clinical Medicine, Magna Graecia University of Catanzaro, Salvatore Venuta University Campus, Catanzaro, Italy

²Laboratory of Molecular Oncology, Department of Experimental and Clinical Medicine, Magna Graecia University, Catanzaro, Italy, CIS for Genomics and Molecular Pathology, Magna Graecia University, Catanzaro, Italy

³Stem Cell Laboratory, Research Center of Advanced Biochemistry and Molecular Biology, Department of Experimental and Clinical Medicine University "Magna Graecia" of Catanzaro, Salvatore Venuta University Campus, Catanzaro, Italy

*Co-first authors

#Co-senior authors

Correspondence to: Domenica Scumaci; email: Scumaci@unicz.it

Keywords: breast cancer, histone, 2D TAU gel, phosphorylation, FAK

Received: March 25, 2019

Accepted: November 26, 2019

Published: December 8, 2019

Copyright: Perri et al. This is an open-access article distributed under the terms of the Creative Commons Attribution License (CC BY 3.0), which permits unrestricted use, distribution, and reproduction in any medium, provided the original author and source are credited.

ABSTRACT

Histones and their variants are subjected to several post-translational modifications (PTMs). Histones PTMs play an important role in the regulation of gene expression and are critical for the development and progression of many types of cancer, including breast cancer. In this study, we used two-dimensional TAU/SDS electrophoresis, coupled with mass spectrometry for a comprehensive profiling of histone PTMs in breast cancer cell lines. Proteomic approach allowed us to identify 85 histone PTMs, seventeen of which are not reported in the UniProt database. Western blot analysis was performed to confirm a peculiar pattern of PTMs in the sporadic and hereditary breast cancer cell lines compared to normal cells. Overlapping mass spectrometry data with western blotting results, we identified, for the first time to our knowledge, a tyrosine phosphorylation on histone H1, which is significantly higher in breast cancer cells. Additionally, by inhibiting specific signaling paths, such as PI3K, PPAR γ and FAK pathways, we established a correlation between their regulation and the presence of new histone PTMs. Our results may provide new insight on the possible implication of these modifications in breast cancer and may offer new perspectives for future clinical applications.

INTRODUCTION

In eukaryotic cells, DNA is packaged into chromatin. The level of compaction derives from the degree of DNA winding around nucleosomes [1]. Each nucleosome consists of 147bp of DNA wrapped around an octamer core containing one histone H3–H4 tetramer and two histone H2A–H2B dimers. Histones are very basic proteins highly conserved throughout evolution,

organized in three domains: the hydrophobic central globular domain that interacts with DNA, and the very basic unstructured C- and N-terminal tails [2, 3]. Tails protrude away from the nucleosome and are frequently subjected to post-translational modifications (PTMs). In addition to histones of the core particle, the linker histone H1 binds the DNA on the surface of the nucleosomal core and completes the nucleosome. The histone linker is required to stabilize the highly ordered chromatin

structure [4]. The action of H1 histone influences the nucleosomal repeat length (NRL), thereby modulating the accessibility of chromatin for transcription [2, 4].

The degree of packaging of chromatin is highly influenced by numerous factors, including histone PTMs [1]. Enzymes called *writers* and *erasers* add and remove PTMs from histones, affecting inter/intra-nucleosomal interactions and their binding to DNA. In addition, histone readers specifically bind certain PTMs, resulting in specific responses at the level of transcription, DNA repair and replication [3].

Histones and histone-variants represent a key class of proteins able to trigger the encoding of epigenetic information as well as the regulation of gene expression [5]. Histone PTMs profiles (histone code) are known to be altered in many types of cancer, including breast cancer, the most frequent neoplasia among women. Specific histone PTMs are associated with breast cancer development and prognosis, such as H3K9ac, H3K9me2-3, H4K16ac and H4K20me3 [3, 6–10]. A plethora of studies suggests a pivotal role of histone modifications in the onset as well as in the progression of breast cancer. Therefore, profiling and characterization of histone isoforms and their PTMs may contribute to unravel the molecular mechanisms underlying breast tumorigenesis. Moreover, the role of epigenetics in sporadic as well as in hereditary breast cancer needs to be deepened in order to provide novel targets for the development of personalized therapeutic approaches.

In this work, we applied 2D-TAU/SDS gel electrophoresis coupled to LC-MS/MS analysis to identify and characterize histone PTMs profiles in normal mammary epithelial cell line MCF10 and in two distinct breast cancer cell lines: MCF7 (sporadic breastcancer model) and HCC1937 (*BRCA1*^{-/-} hereditary breast cancer model) [11–14].

Seventeen novel histone marks were identified. In addition, 2D-TAU Western blot analysis was applied to differentially profile the tyrosine phosphorylation pattern in all cell lines.

The most striking result is the identification of a tyrosine phosphorylation on the histone H1, that increases in breast cancer cells and correlates with the proliferative status. To the best of our knowledge, this is the first report of such a finding.

Ultimately, we identify additional putative cancer-related histone marks, we reveal quantitative differences of PTMs in different cellular models of breast cancer and, suggesting a pivotal role of these modifications in proliferation, we provide a substantial input for further investigations.

RESULTS

2D TAU gel of histone PTMs in breast cell lines

Histones were isolated from mammalian cell lines and proteins content was determined using Bradford Protein Assay (Bio-Rad) according to the manufacturer's instructions with human serum albumin (Sigma Aldrich) as standard. Twenty µg of each sample were loaded on a 1D TAU-gel to assess the efficiency of the isolation methods. The gel, relative to the separation of histones is shown in Figure 1A. As expected, the separation pattern of histone isoforms was found coherent with previous literature [11].

Two-dimensional (2D) TAU gel allowed us to resolve each histone isoform. Gel maps are shown as Figure 1B. By means of this approach, we obtained a map of thirteen protein spots. Images analysis, performed using image master 2d platinum software, allows us to focus specifically on the histone isoforms differentially expressed in cancer cells compared to normal cells. Differentially expressed histone spots are marked with a progressive number on the 2D gel map.

Mass spectrometry analysis of TAU gel spot reveals novel PTMs in breast cancer cells

Gel spots were in-gel digested with trypsin and analyzed by mass spectrometry. Table 1 summarizes the results of the LC-MS/MS identifications. For each identification, we reported accession number, number of identified peptides and percentage of sequence coverage. As expected, each protein spot corresponded to a specific histone isoform. As shown in Figure 2, we identified several modifications on all the five canonical histones. Among these, some had been previously reported in the UniProt database (<http://www.uniprot.org>), many others were novel. PTMs we found consist of lysine acetylation, lysine and arginine methylation, dimethylation, trimethylation, arginine citrullination and threonine, tyrosine and serine phosphorylation.

As summarized in Figure 2A we identified a total of eighty-five histones PTMs, 17 of which not previously described on the UniProt database. Figure 2B–2C lists all histone isoforms PTMs identified in this study. MS/MS data are provided as Supplementary Figure 3.

Western blot analysis of specific histone PTMs in breast cancer cell lines

Our analytic procedure was validated by analyzing, through western blot experiment, the expression of specific histone PTMs known to be dysregulated in breast cancer.

The availability of commercial antibodies to specific sites allowed us to highlight important differences between the normal mammary epithelial cell line and breast cancer cell lines.

Western blot analysis was done on four histone marks: H4K16ac, H3K9ac, H4K20me3 and H3K9me2-3. Expression of each modification is shown in Figure 3A.

The dysregulation of peculiar histone marks was observed in both cancer cells (MCF7 and HCC1937) compared to normal cells (MCF10).

We found low levels of H4K16ac and H4K20me3, fully in agreement with current literature that links aberrant low levels of these modifications with cell invasiveness, and breast cancer progression [9, 10]. We also detected in our cancer cells high levels of H3K9me2-3, enforcing the notion that the epigenetic silencing of several tumor suppressor genes is a key event in breast cancer cells [15, 17].

As expected, the levels of H3K9ac was low being methylation and acetylation mutually exclusive [17, 18].

A key regulator of H3K9 acetylation is the NAD-dependent histone deacetylase SIRT1 that is overexpressed in many types of cancer including breast cancer. SIRT1 plays an important role in several cellular processes such as chromatin assembly, gene transcription and inflammation. Usually, the enzyme is able to act on two groups of acetylated proteins: histone and non-histone proteins. For histone targets, the status of acetylation/deacetylation determines whether chromatin is accessible for gene transcription. SIRT1 directly deacetylates H1K26, H3K9, and H4K16 and influences DNA compaction, silencing gene transcription [19]. We performed Western blot analysis of total SIRT1 levels in whole protein extracts from MCF10, MCF7 and HCC1937 cells. Consistently, levels of SIRT1 were significantly increased in breast cancer cells compared to normal mammary epithelial cells as shown in Figure 3B.

Tyrosine phosphorylation profiling of histones by 2D Western Blot analysis

The overall pattern of histone tyrosine phosphorylation of all three cellular models was analyzed by 2D TAU gel,

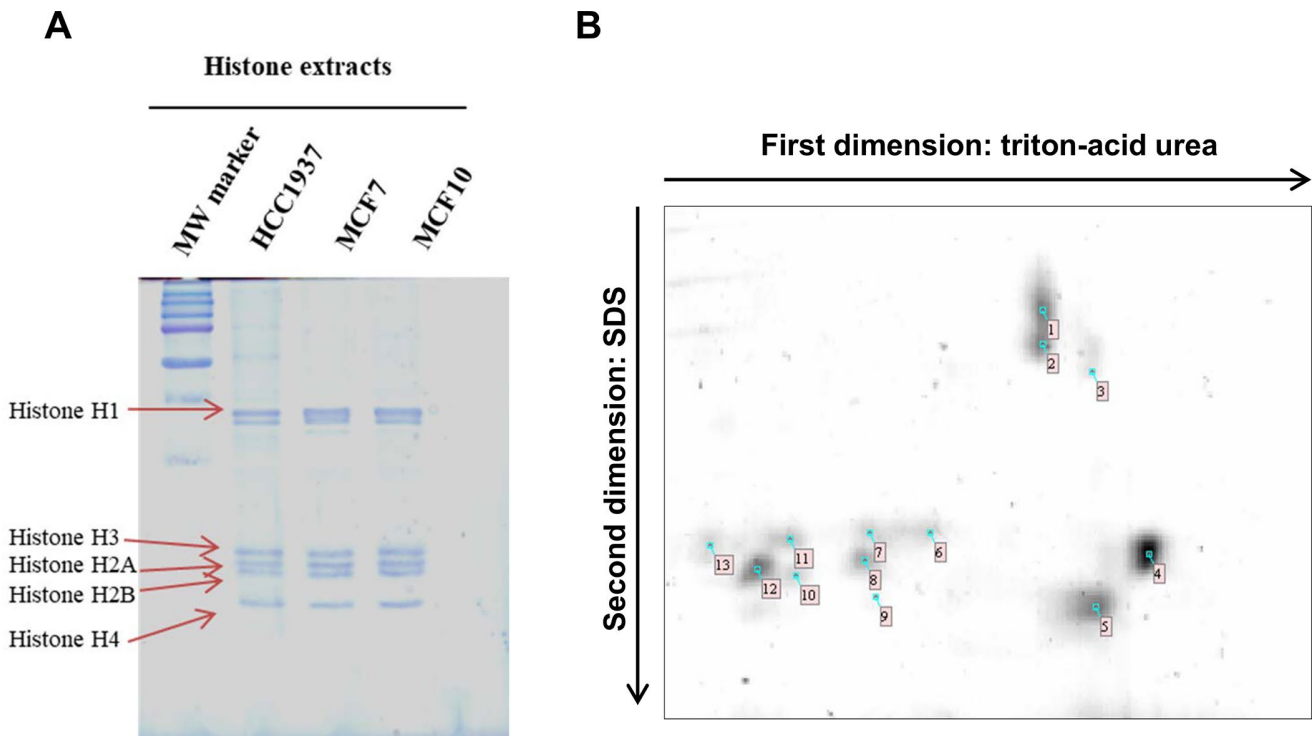


Figure 1. 1D TAU gel and 2D TAU gel map of histones in breast cancer cells. (Panel A) The image shows a peculiar separation pattern of histone isoforms, extract from HCC1937, MCF7 and MCF10 cells lines, using 1D-TAU gel. (Panel B) Representative 2D TAU PAGE of histones extract from MCF7 cells. Histones were first resolved by TAU gel and subsequently separated using SDS gel. Spots extracted and analyzed by mass spectrometry are noted on the gel map. All experiments were repeated three times using biologic replicates. Numbered spots are described on table 1 where for each spot is reported the id number, the accession number, histone description, the number of identified peptides, the percentage of sequence coverage, molecular weight and isoelectric point.

Table 1. LC-MS/MS identifications.

Spot id	Accession number	Description	Coverage	Unique Peptides	Score	MW [kDa]	calc. pI
Spot 1	P16401	Histone H1.5 OS=Homo sapiens GN=HIST1H1B PE=1 SV=3 - [H15_HUMAN]	35,84	12	237,42	22,6	10,92
Spot 2	P16403	Histone H1.2 OS=Homo sapiens GN=HIST1H1C PE=1 SV=2 - [H12_HUMAN]	34,74	12	390,76	21,4	10,93
	P16402	Histone H1.3 OS=Homo sapiens GN=HIST1H1D PE=1 SV=2 - [H13_HUMAN]	35,29	11	229,94	22,3	11,02
Spot 3	P07305	Histone H1.0 OS=Homo sapiens GN=H1F0 PE=1 SV=3 - [H10_HUMAN]	50,00	13	92,32	20,9	10,84
	P07305-2	Isoform 2 of Histone H1.0 OS=Homo sapiens GN=H1F0 - [H10_HUMAN]	33,33	8	155,68	19,2	10,83
Spot 4	Q5QNW6	Histone H2B type 2-F OS=Homo sapiens GN=HIST2H2BF PE=1 SV=3 - [H2B2F_HUMAN]	80,95	6	719,93	13,9	10,32
	P06899	Histone H2B type 1-J OS=Homo sapiens GN=HIST1H2BJ PE=1 SV=3 - [H2B1J_HUMAN]	79,37	3	691,82	13,9	10,32
	O60814	Histone H2B type 1-K OS=Homo sapiens GN=HIST1H2BK PE=1 SV=3 - [H2B1K_HUMAN]	41,27	6	30,84	13,9	10,32
	P58876	Histone H2B type 1-D OS=Homo sapiens GN=HIST1H2BD PE=1 SV=2 - [H2B1D_HUMAN]	80,95	4	943,16	13,9	10,32
	P23527	Histone H2B type 1-O OS=Homo sapiens GN=HIST1H2BO PE=1 SV=3 - [H2B1O_HUMAN]	80,95	3	630,95	13,9	10,32
	Q99880	Histone H2B type 1-L OS=Homo sapiens GN=HIST1H2BL PE=1 SV=3 - [H2B1L_HUMAN]	73,81	4	255,71	13,9	10,32
	Q8N257	Histone H2B type 3-B OS=Homo sapiens GN=HIST3H2BB PE=1 SV=3 - [H2B3B_HUMAN]	73,81	4	223,44	13,9	10,32
Spot 5	P62805	Histone H4 OS=Homo sapiens GN=HIST1H4A PE=1 SV=2 - [H4_HUMAN]	84,47	19	1058,19	11,4	11,36
Spot 6	P68431	Histone H3.1 OS=Homo sapiens GN=HIST1H3A PE=1 SV=2 - [H31_HUMAN]	62,5	14	144,31	15,4	11,12
Spot 7	Q71DI3	Histone H3.2 OS=Homo sapiens GN=HIST2H3A PE=1 SV=3 - [H32_HUMAN]	83,82	3	380,59	15,4	11,27
	K7EK07	Histone H3 (Fragment) OS=Homo sapiens GN=H3F3B PE=3 SV=1 -	65,91	4	196,58	14,9	11,30

		[K7EK07_HUMAN]					
	P68431	Histone H3.1 OS=Homo sapiens GN=HIST1H3A PE=1 SV=2 - [H31_HUMAN]	63,97	4	333,96	15,4	11,12
Spot 8	Q16777	Histone H2A type 2-C OS=Homo sapiens GN=HIST2H2AC PE=1 SV=4 - [H2A2C_HUMAN]	63,57	7	136,64	14,0	10,90
	Q96KK5	Histone H2A type 1-H OS=Homo sapiens GN=HIST1H2AH PE=1 SV=3 - [H2A1H_HUMAN]	58,59	5	108,22	13,9	10,89
Spot 9	P0C0S5	Histone H2A.Z OS=Homo sapiens GN=H2AFZ PE=1 SV=2 - [H2AZ_HUMAN]	31,25	2	37,33	13,5	10,58
Spot 10	Q96KK5	Histone H2A type 1-H OS=Homo sapiens GN=HIST1H2AH PE=1 SV=3 - [H2A1H_HUMAN]	79,69	3	224,94	13,9	10,89
	Q93077	Histone H2A type 1-C OS=Homo sapiens GN=HIST1H2AC PE=1 SV=3 - [H2A1C_HUMAN]	78,46	2	222,63	14,1	11,05
Spot 11	P68431	Histone H3.1 OS=Homo sapiens GN=HIST1H3A PE=1 SV=2 - [H31_HUMAN]	63,97	20	587,61	15,4	11,12
Spot 12	Q96KK5	Histone H2A type 1-H OS=Homo sapiens GN=HIST1H2AH PE=1 SV=3 - [H2A1H_HUMAN]	79,69	3	224,94	13,9	10,89
	P16104	Histone H2A.x OS=Homo sapiens GN=H2AFX PE=1 SV=2 - [H2AX_HUMAN]	65,03	2	104,67	15,13	10,74
	P0C0S5	Histone H2A.Z OS=Homo sapiens GN=H2AFZ PE=1 SV=2 - [H2AZ_HUMAN]	56,25	4	116,77	13,5	10,58
	Q93077	Histone H2A type 1-C OS=Homo sapiens GN=HIST1H2AC PE=1 SV=3 - [H2A1C_HUMAN]	78,46	2	222,64	14,1	11,05
	Q8IUE6	Histone H2A type 2-B OS=Homo sapiens GN=HIST2H2AB PE=1 SV=3 - [H2A2B_HUMAN]	60,00	3	75,51	14,0	10,89
Spot 13	K7EK07	Histone H3 (Fragment) OS=Homo sapiens GN=H3F3B PE=3 SV=1 - [K7EK07_HUMAN]	63,64	4	183,74	14,9	11,30
	P68431	Histone H3.1 OS=Homo sapiens GN=HIST1H3A PE=1 SV=2 - [H31_HUMAN]	61,76	4	155,95	15,4	11,12
	Q71DI3	Histone H3.2 OS=Homo sapiens GN=HIST2H3A PE=1 SV=3 - [H32_HUMAN]	85,29	5	339,42	15,4	11,27

In the table are summarized the results of the LC-MS/MS identifications. For each identification, we reported the number by which spot are marked on Figure 1, the accession number, the number of identified peptides and the % of sequence coverage. Mass spectrometry data are averages of three biologic replicates.

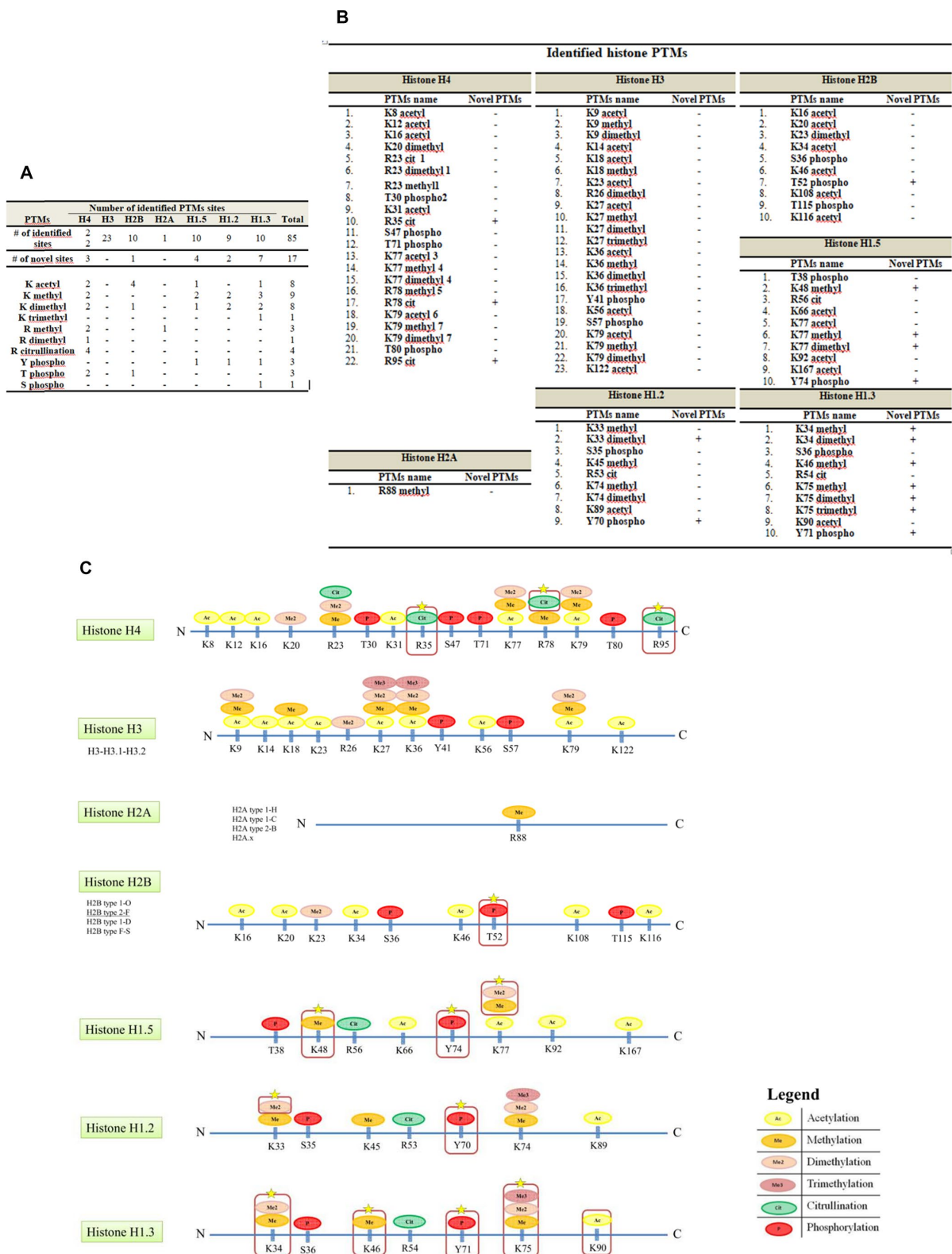


Figure 2. Histone PTMs sites identified by this study. (A) The table summarizes all the PTMs sites identified. Using the described approach, we identified a total of eighty-five histones PTMs, seventeen of these were not previously described on the UniProt database. (B) The identified novel modifications consist of 5 lysine methylation, 4 lysine dimethylation, 1 lysine trimethylation, 3 arginine citrullination, 1 threonine phosphorylation and 3 tyrosine phosphorylation. Mass spectrometry data are averages of three biologic replicates. (C) Novel and known sites of PTM along histones sequences. The identified modifications consist of acetylation, methylation, dimethylation, trimethylation, citrullination and phosphorylation. Red boxes indicate novel modifications.

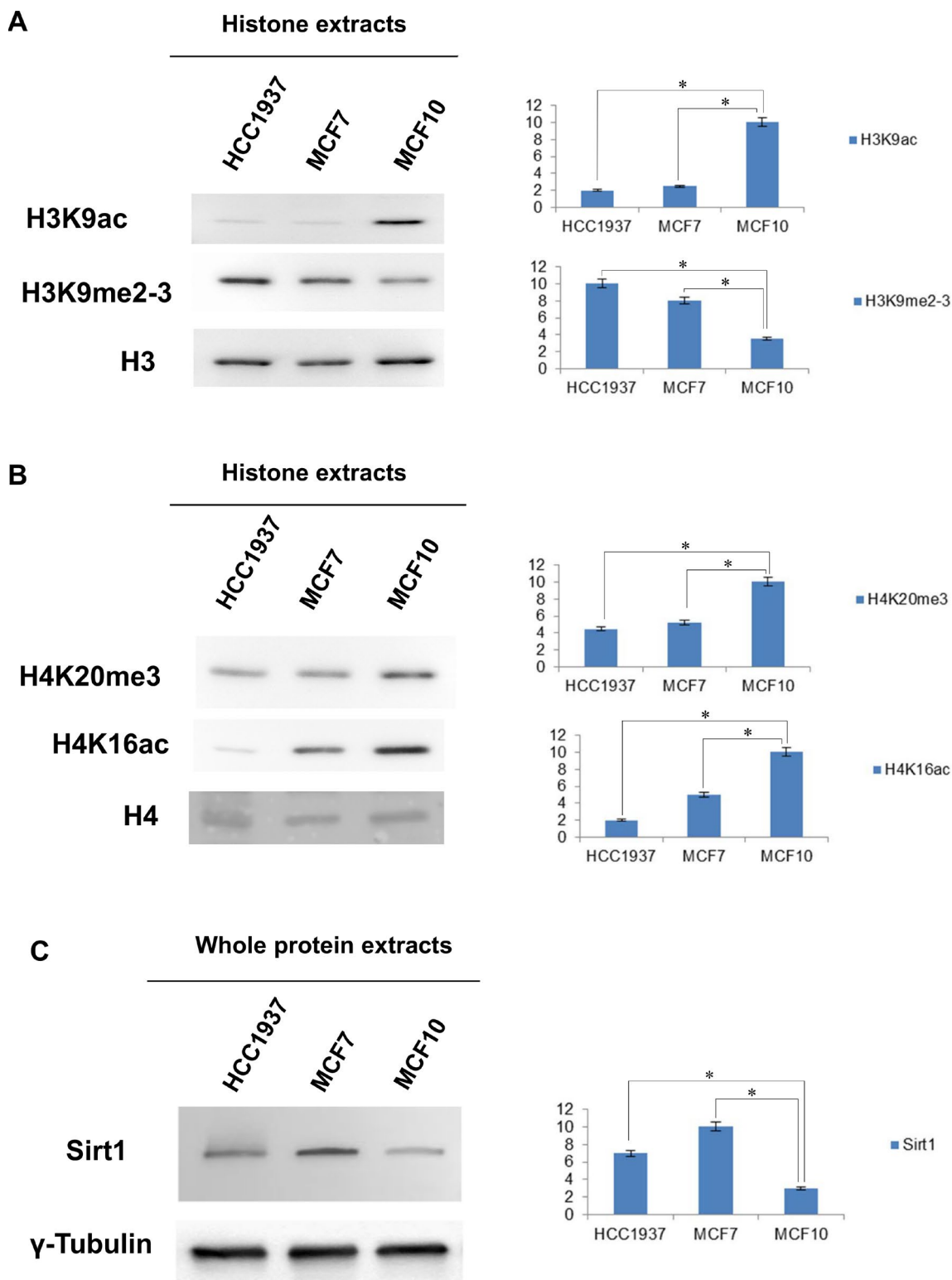


Figure 3. Western blot and densitometry analysis relative to the expression of histone marks and SIRT1 in MCF10, MCF7 and HCC1937 cells. (A) Western blot and densitometry analysis relative to the expression of histone marks in MCF10, MCF7 and HCC1937 cells. (A) H3K9ac, H3K9me2-3, PMTs signal were normalized against the total level of histone H3. (B) H4K20me3, H4K16Ac, PMTs signal were normalized against the total level histone H4. (C) Western blot and densitometry analysis of the expression levels of SIRT1 in whole protein extracts from MCF10, MCF7 and HCC1937 cells. A goat polyclonal anti- γ -Tubulin antibody was used (C-20) to confirm an equal loading of proteins. The assays were repeated in three independent biological replicates and statistically significant differences were determined using one-way ANOVA followed by Dunnett's multiple comparisons test. Data are expressed as mean \pm SEM (N =3), p-value <0.05.

followed by Western blotting with anti-phospho-Y antibodies. Figure 4 illustrates the tyrosine phosphorylation patterns. In panel A are shown representative images of 2D TAU Western blot, and in the panel B is reported the corresponding densitometry analysis. The most significant finding is the detection of a phosphorylation in tyrosine on the histone H1.

H1 histone tyrosine phosphorylation results increased in breast cancer cell lines

Mass spectrometry analysis revealed three sites of tyrosine phosphorylation, at Y74 on H1.5, at Y70 on H1.2 and at Y71 on H1.3 respectively, relative MS/MS spectra are reported in Figure 5. Interestingly, these

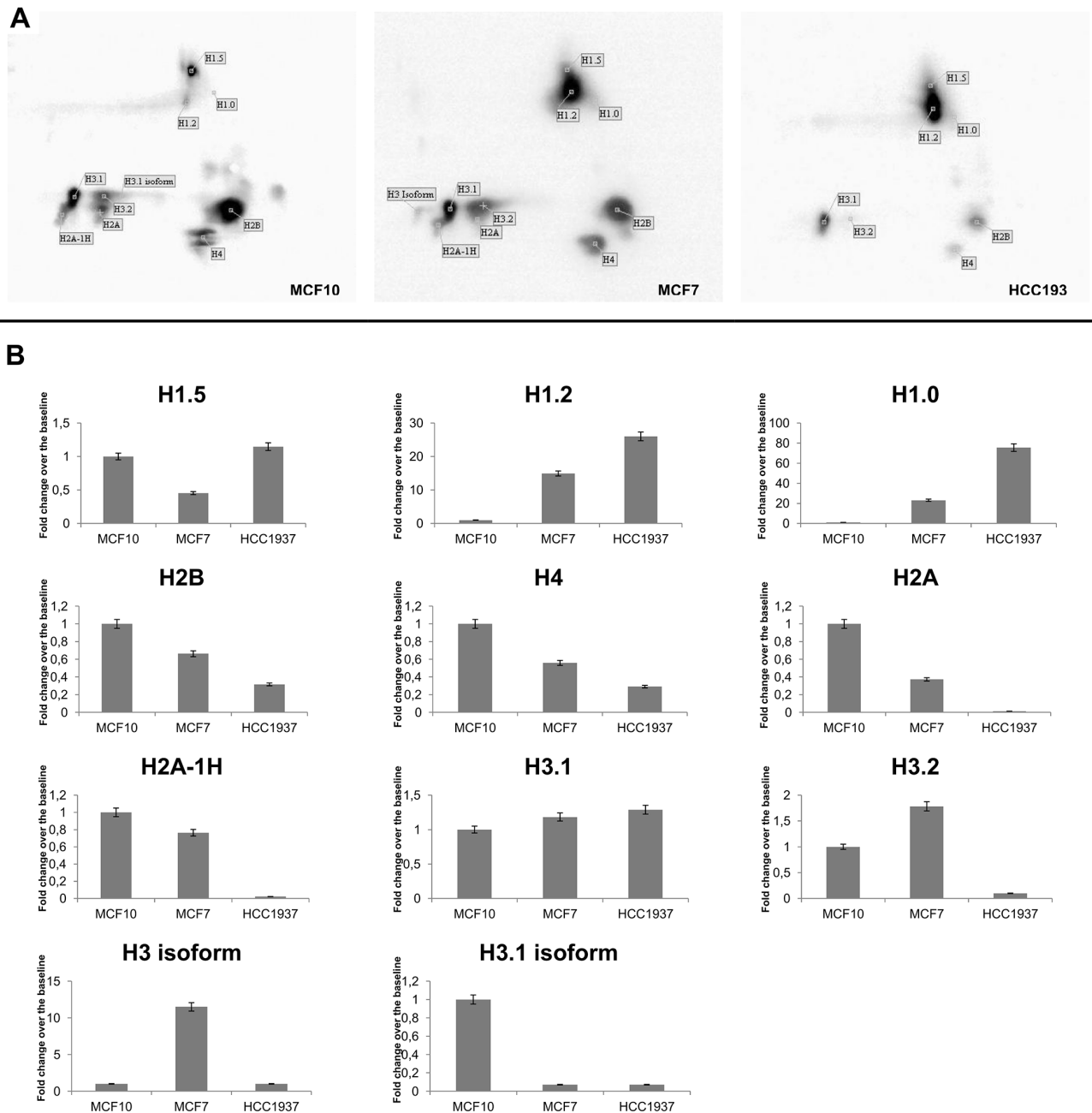
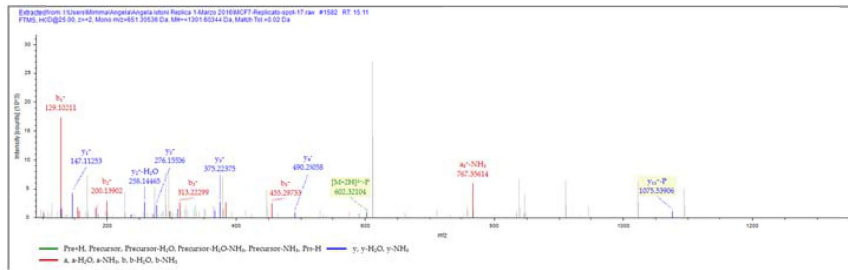


Figure 4. Tyrosine phosphorylation profiling of histones by 2D Western Blot analysis. 2D TAU Western blot of histone tyrosine phosphorylation pattern (panel A) and densitometry analysis of differentially expressed spots (panel B). The assay was repeated in three independent biological replicates; statistical analysis was done by one-way ANOVA, followed by Dunnett's multiple comparisons test. Differences were considered significant when $P \leq 0.05$ (*). Data are expressed as mean \pm SEM (N =3). Images relative to proteins normalization are provided as Supplementary Figure 2.

A KALAAGGY_{Phospho}DVEK

H1.5Y74

Sequence: KALAAGGYDVEK, Y8-Phospho (79.96633 Da)
 Charge: +2, Monoisotopic m/z: 651.30536 Da (-5.17 mmu/-7.94 ppm), MH+: 1301.60344 Da, RT: 15.11 min,
 Identified with: Sequest HT (v1.3); XCorr:1.67, Ions matched by search engine: 0/0
 Fragment match tolerance used for search: 0.02 Da

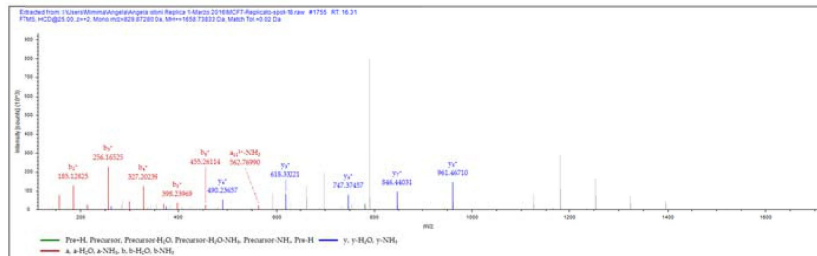


#1	a*	a2*	b*	b2*	Seq.	y*	y2*	#2
1	101.10733	51.05730	129.10225	65.05476	K			12
2	172.14445	86.57586	200.13937	100.57332	A	1173.51880	587.26304	11
3	285.22852	143.11790	313.22344	157.11536	L	1102.48168	551.74448	10
4	356.26564	178.63646	384.26056	192.63392	A	989.39761	495.20244	9
5	427.30276	214.15502	455.29768	228.15248	A	918.36049	459.68388	8
6	484.32423	242.66575	512.31915	256.66321	G	847.32337	424.16532	7
7	541.34570	271.17649	569.34062	285.17395	G	790.30190	395.65459	6
8	784.37535	392.69131	812.37027	406.68877	Y-Phospho	733.28043	367.14385	5
9	899.40230	450.20479	927.39722	464.20225	D	490.25078	245.62903	4
13	998.47072	499.73900	1026.46564	513.73646	V	375.22383	188.11555	3
11	1127.51332	564.26030	1155.50824	578.25776	E	276.15541	138.58134	2
12					K	147.11281	74.06004	1

B ALAAAGY_{Phospho}DVEKNSR

H1.2Y70 – H1.3Y71

Sequence: ALAAAGYDVEKNSR, Y7-Phospho (79.96633 Da)
 Charge: +2, Monoisotopic m/z: 829.87280 Da (-7.57 mmu/-9.12 ppm), MH+: 1658.73833 Da, RT: 16.31 min,
 Identified with: Sequest HT (v1.3); XCorr:2.90, Ions matched by search engine: 0/0
 Fragment match tolerance used for search: 0.02 Da



#1	a*	a2*	b*	b2*	Seq.	y*	y2*	#2
1	44.04948	22.52838	72.04440	36.52584	A			15
2	157.13355	79.07041	185.12847	93.06787	L	1587.71634	794.36181	14
3	228.17067	114.58897	256.16559	128.58643	A	1474.63227	737.81977	13
4	299.20779	150.10753	327.20271	164.10499	A	1403.59515	702.30121	12
5	370.24491	185.62609	398.23983	199.62355	A	1332.55803	666.78265	11
6	427.26638	214.13683	455.26130	228.13429	G	1261.52091	631.26409	10
7	670.29603	335.65165	698.29095	349.64911	Y-Phospho	1204.49944	602.75336	9
8	785.32298	393.16513	813.31790	407.16259	D	961.46979	481.23853	8
9	884.39140	442.69934	912.38632	456.69680	V	846.44284	423.72506	7
10	1013.43400	507.22064	1041.42892	521.21810	E	747.37442	374.19085	6
11	1141.52897	571.26812	1169.52389	585.26558	K	618.33182	309.66955	5
12	1255.57190	628.28959	1283.56682	642.28705	N	490.23685	245.62206	4
13	1369.61483	685.31105	1397.60975	699.30851	N	376.19392	188.60060	3
14	1456.64686	728.82707	1484.64178	742.82453	S	262.15099	131.57913	2
15					R	175.11896	88.06312	1

Figure 5. Fragmentation MS/MS spectra. (Panel A) Fragmentation MS/MS spectra of the modified peptide carrying the novel PTMs. MS/MS data are referred to histone H1.5. Data were analyzed by Proteome Discoverer 1.4 software. MS/MS data were searched on the Human UniProt database. False discovery rate (FDR) of peptide identifications was estimated using the “Target-decoy PSM validator” node in Proteome Discoverer. Cut off filters 95% confidence and a minimum of two peptide identifications per protein. (Panel B) Fragmentation MS/MS spectra of the modified peptide carrying the novel PTMs. MS/MS data are referred to histones H1.2 and H1.3. Data were analyzed by

Proteome Discoverer 1.4 software. MS/MS data were searched on the Human UniProt database. False discovery rate (FDR) of peptide identifications was estimated using the “Target-decoy PSM validator” node in Proteome Discoverer. Cut off filters 95% confidence and a minimum of two peptide identifications per protein.

sites are located in the highly conserved central globular domain of histone H1 [4].

To quantify the expression level of this peculiar PTM, we coupled 2D TAU Western blot with the anti-whole phospho-tyrosine antibody staining, considering that 2D TAU Western blot is able to resolve each H1 variants in a single spot and that H1 isoforms have a single tyrosine residue in their sequence as found by serendipity analysis.

Levels of tyrosine phosphorylation in H1 variants were significantly higher in breast cancer cells compared to normal cells suggesting a role of these modifications in breast cancer (Figure 6, panel A).

LY294002, Troglitazone and PND1186 treatments reduce levels of H1 tyrosine phosphorylation in sporadic breast cancer cell lines

Recently, a paper, focused on global survey of phosphotyrosine signaling in lung cancer linked tyrosine histone phosphorylation with cellular proliferation [20].

In order to shed more light into biology of H1 tyrosine phosphorylation and to define correlations with cancer phenotype and progression, we carried out a set of experiments in which mitogenic pathways had been pharmacologically modulated.

Cell proliferation induced by recombinant epidermal growth factor (rEGF) produced in both normal and breast cancer cells, an increased tyrosine phosphorylation of H1, more evident in tumoral cells (MCF7) compared to normal cells (MCF10) (Figure 6, panel B and C).

Consistently, treatment by LY294002, a specific PI3K inhibitor [21, 22] and troglitazone (TGZ), a PPAR γ agonist, known to exhibit anti-proliferative activity in breast cancer cells [23–25] both achieved a significant reduction of H1 tyrosine phosphorylation in MCF7 (Figure 7, panel A and B). Impaired tyrosine phosphorylation levels on H1 were assessed by 2D Western blot mapping.

Once tyrosine phosphorylation was correlated with proliferation, the *in silico* tool Phosphonet (<http://www.phosphonet.ca>) was used to analyze the consensus of histone that encloses phosphorylated tyrosine. Phosphonet database allows us to assess, that

phosphosite Y74 of histone H1.5; Y70 of H1.2 and at Y71 of H1.3 were putative consensus of the Focal Adhesion Kinase (FAK), a tyrosine kinase capable of nuclear localization [26, 28]. To define its role in our system, we modulated FAK activity by a specific inhibitor, PND1186. PND1186, also known as VS-4718, is a reversible FAK inhibitor with an IC₅₀ value of 100 nM in breast carcinoma cells [29, 30].

Interestingly at 1 hour FAK inhibition induced a remarkable reduction of H1 tyrosine phosphorylation (Figure 8A). We performed a time course analysis and, as shown in Figure 8F, downregulation of H1 tyrosine phosphorylation had a timing suggestive of an involvement of FAK in controlling and/or catalyzing the reaction.

A cell proliferation assay allowed us to formalize the activity of PND1186 on (MCF7) proliferation of breast cancer cells. As shown in Figure 8G FAK inhibition decreases cell proliferation in a time dependent manner.

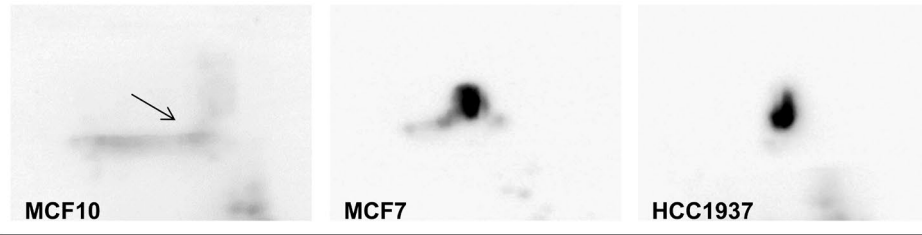
LY294002, Troglitazone and PND1186 treatments reduce levels of H1 tyrosine phosphorylation in hereditary breast cancer cell lines

The effects of LY294002, Troglitazone and PND1186 drugs were also assessed in HCC1937 breast cancer cells, a model of hereditary breast cancer. As shown in Figure 9, panel A, B and C, the three molecules are able to induce a significant reduction of H1 tyrosine phosphorylation levels not differently from what we observed in the sporadic model.

Immunoprecipitation analysis reveals an interaction between nuclear FAK and histone H1

The ability of FAK to directly interact with the histone H1 was investigated by co-immunoprecipitation experiments. We incubated the nuclear protein extract from MCF10, MCF7 and HCC1937 cells with an anti-FAK antibody. The immunoprecipitated fraction was assayed with antibodies against histone H1 and pFAK. Interestingly pFAK and Histone H1 co-immunoprecipitated, demonstrating that pFAK and H1 are potentially capable of a direct interaction (Figure 10). The levels of FAK in whole and nuclear extracts are shown in Figure 10A; Vimentin blot was used to assess that nuclear extracts are not contaminated by cytoplasmic fraction.

Panel A: H1 phospho-Tyrosine



Panel B: EGF treatment

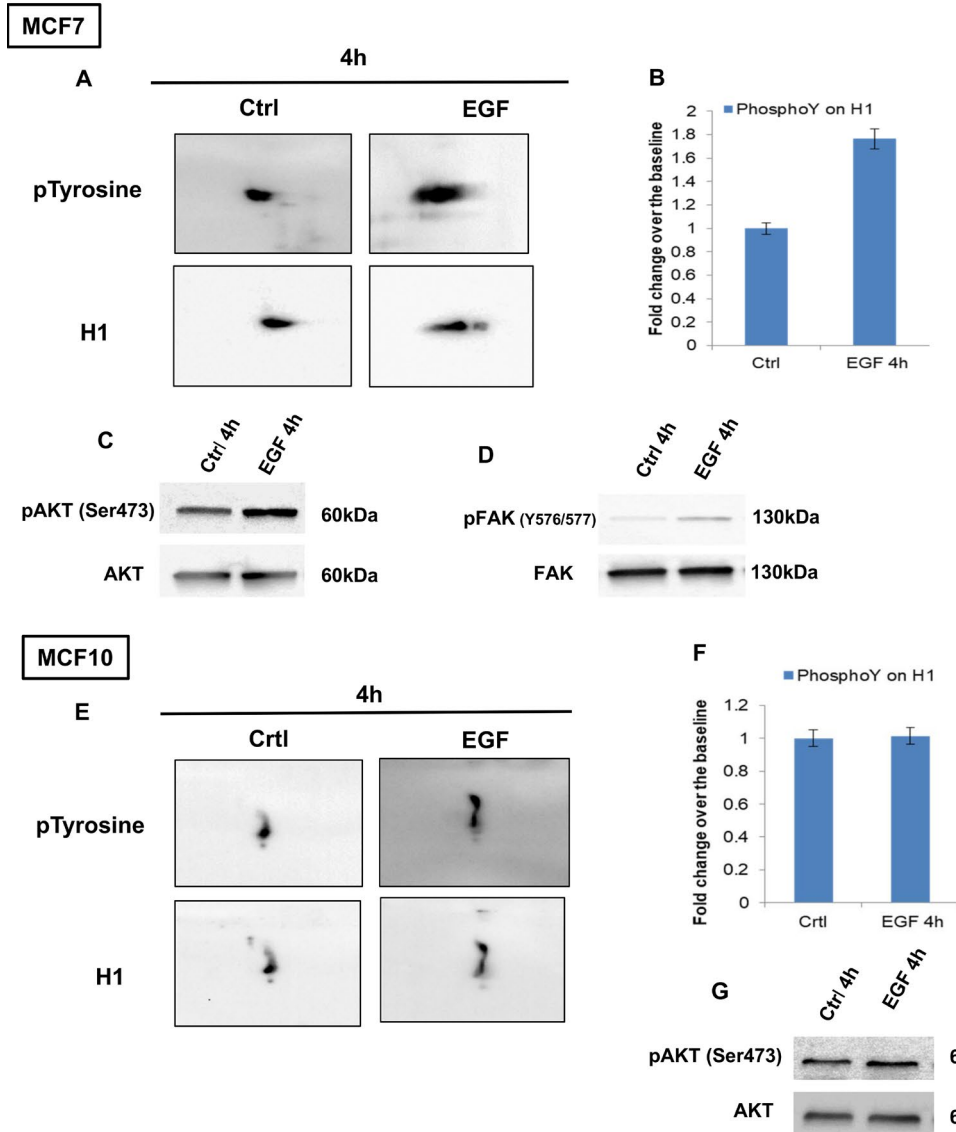
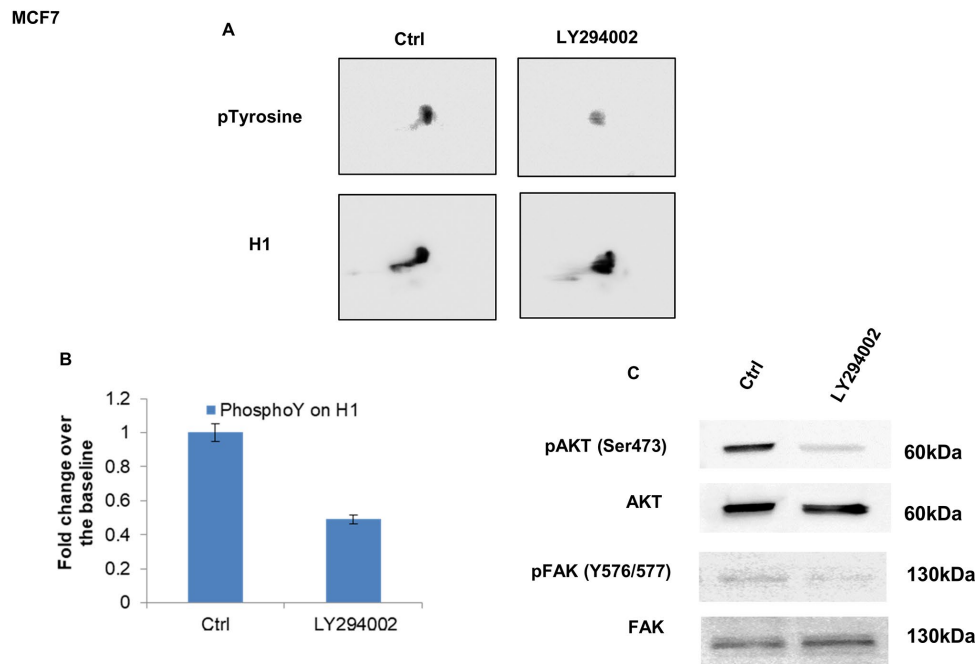


Figure 6. Analysis of H1 histone tyrosine phosphorylation in breast and normal cancer cells, using 2D-TAU western blot. (Panel A) 2D western blots showing tyrosine phosphorylation on the Histone H1 in MCF10, MCF7 and HCC1937 cells. Arrow indicates the region corresponding to the phosphorylated protein. Blot images were acquired using Alliance 2.7 (UVITEC, Eppendorf, Milan, Italy). Membranes signals were acquired concomitantly at 4 seconds. (Panel B) (A) 2D TAU western blot analysis of histone H1 tyrosine phosphorylation on MCF7 cells (acquisition time: 4'') and (E) MCF10 cells (acquisition time: 20'') following EGF stimulation. Lower panels indicate the relative normalization with H1 antibody; the relative densitometry analyses are shown in B for MCF7 cells and in F for MCF10 cell lines. The assays were repeated in three independent biological replicates Data are expressed as mean \pm SEM (N =3). (C, G): Western blot analysis of pAKT and AKT levels on whole protein extracts from EGF treated MCF7 and MCF10 cells, respectively. (D) Western blot analysis of pFAK (Y576/577) levels on whole protein extracts from EGF treated MCF7.

Panel A: LY294002 treatment



Panel B: Troglitazone treatment

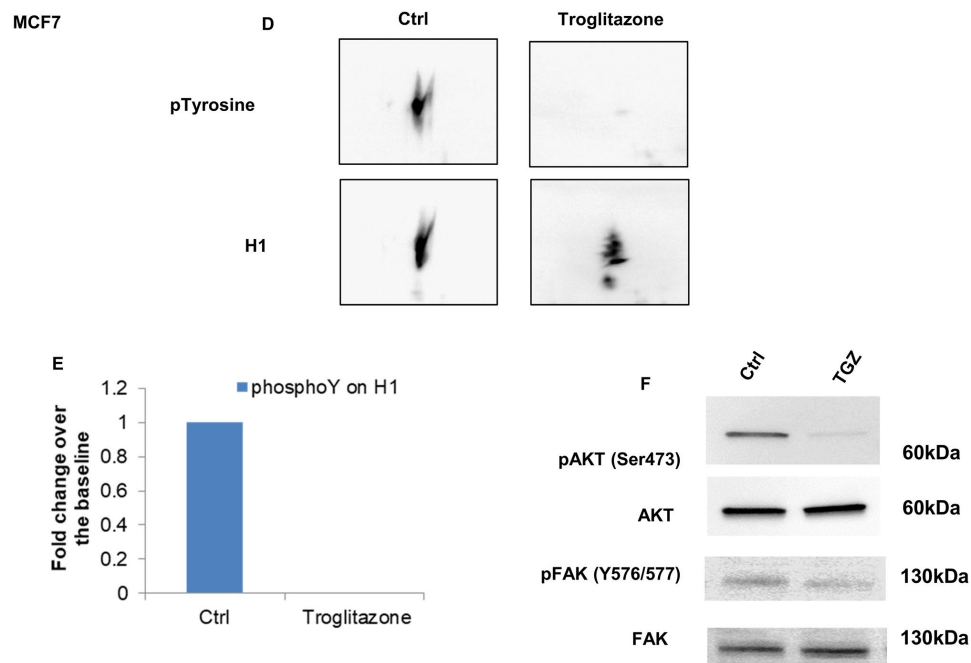


Figure 7. Analysis of H1 histone tyrosine phosphorylation following LY294002 and Troglitazone treatments in MCF7 cells. (Panel A) (A) 2D TAU Western blot analysis of histone H1 tyrosine phosphorylation level (upper panel) and relative normalization with H1 antibody (lower panel) after treatment of MCF7 with LY294002; All WB images were acquired in 4 seconds. (B) Densitometry analysis of H1 tyrosine phosphorylation spots; (C) Western blot analysis of pAKT, and pFAK (Y576/577) levels in protein extracts from LY294002 treated cells. Phospho-Akt (ser473) and pFAK (Y576/577) signals were normalized to the corresponding total Akt and total FAK, respectively. (Panel B) (D) 2D TAU Western blot analysis of histone H1 tyrosine phosphorylation level (upper panel) and relative normalization with H1 antibody (lower panel) after treatment of MCF7 with Troglitazone; All WB 2D images were acquired in 4 seconds. (E) Densitometry analysis of H1 tyrosine phosphorylation spots; (F) Western blot analysis of pAKT, and pFAK (Y576/577) levels in protein extract from Troglitazone treated cells. Phospho-Akt (ser473) and pFAK (Y576/577) signals were normalized against the corresponding total Akt and total FAK respectively. The assays were repeated in three independent biological replicates. Data are expressed as mean \pm SEM (N =3).

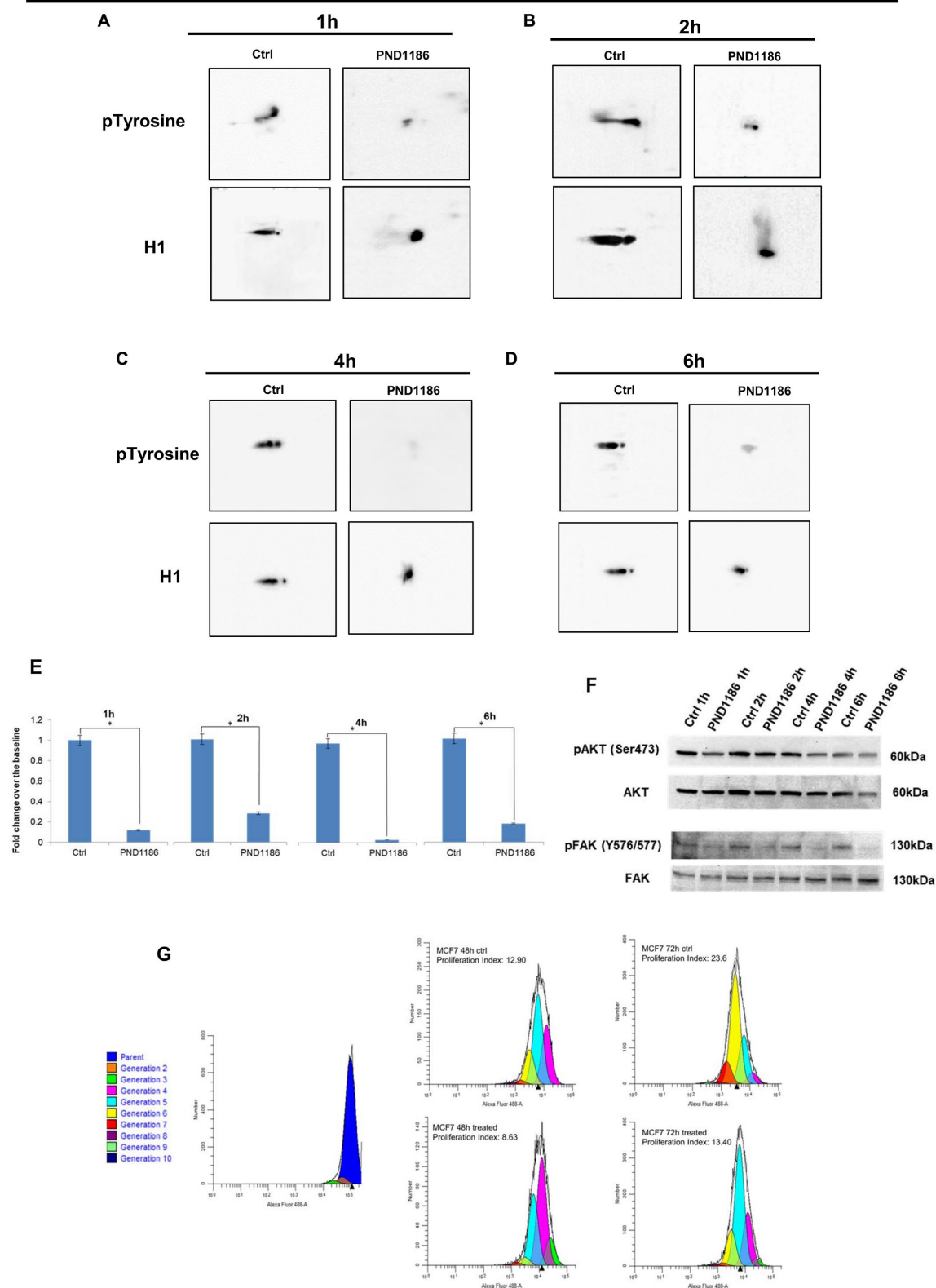


Figure 8. Analysis of H1 histone tyrosine phosphorylation following PND1186 treatments in MCF7 cells. 2D TAU Western blot analysis of histone H1 tyrosine phosphorylation (upper panel) and relative normalization with H1 antibody (lower panel) after PND1186 treatment; a time course of FAK inhibition was done at 1 hour (Panel A), 2 hours (Panel B), 4 hours (Panel C) and 6 hours (Panel D). All WB 2D images were acquired in 4 seconds. (Panel E) Densitometry analysis of H1 tyrosine phosphorylation spots; (panel F) Western blot analysis of

pAKT, and pFAK levels in protein extracts from PND1186-treated cells. Phospho-Akt (ser473) and pFAK (Y576/577) signals were normalized against the corresponding total Akt and total FAK respectively. The assays were repeated in three independent biological replicates. Data are expressed as mean \pm SEM (N =3), (G) Cells untreated and in presence of PND1186 300nM were cultured for 48 and 72 hours. Proliferation potential was detected, at single cell level, by CellTrace™ CFSE labeling. FACS analysis was performed at T₀ (immediately after cell staining to define the parent population) and at 48 and 72 hours. Data were analysed by ModFit LT™ 4.0 software and the proliferation index has been generated for each sample.

Immunofluorescence analysis assess the co-localization of FAK and Histone H1 in the nuclei of proliferating breast cancer cells

To further support the hypothesis of a direct interaction, we investigated the localization of endogenous FAK and histone H1 in the nuclei of MCF7 and HCC1937 cells by immunofluorescence analysis. As expected FAK protein had a predominant cytoplasmic localization, with a weak nuclear signal during the interphase, however FAK strongly marked the mitotic spindle in dividing cells, co-localizing with H1 during metaphase, anaphase and telophase (Figure 11A and 11B). These results, although not conclusive, enforce the hypothesis of a FAK direct involvement in histone H1 phosphorylation.

DISCUSSION AND CONCLUSIONS

Epigenetics plays a key role in physiological processes as well as in the onset and progression of several pathologies. Recently, attention focused on epigenetic phenomena and their association with cancer. Moreover, unlike genetic alterations, epigenetic changes are a reversible phenomenon and therefore potentially druggable [3].

In addition to DNA methylation, histone PTMs are main actors in epigenetic regulation of gene expression. By acting individually or in combination, histone marks modulate the transcriptional state of chromatin and by assembling and disassembling nucleosomes allow or not the binding of transcription factors and ultimately, the building up of the transcriptional machinery.

There are several histone PTMs, with specific biological and pathophysiological implications, whose altered expression has been associated with cancer. Conversely, many other PTMs have roles still unknown.

In our work, we investigated the pattern of histone PTMs in normal and breast cancer cell lines by 2D TAU electrophoresis coupled with mass spectrometry.

The comprehensive analysis of the unmapped PTMs was performed by two-dimensional Western blotting using anti-Y-phospho antibody.

The pattern of PTMs of canonical histones and their variants allowed us to evaluate and to identify

differentially expressed isoforms among the three breast cell types used. Particularly, by overlapping immunoblotting results with mass spectrometry data, we found peculiar tyrosine phosphorylations at residues Y74 of histone H1.5; at Y70 in H1.2 and at Y71 in H1.3.

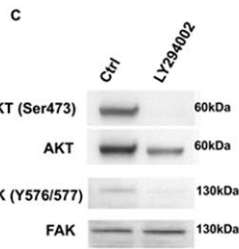
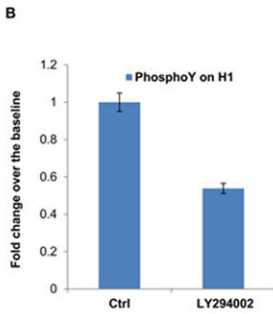
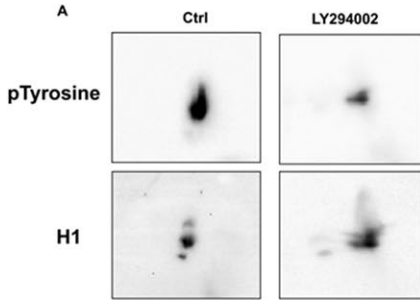
Our data clearly demonstrate that levels of H1 tyrosine phosphorylation are much higher in both the analyzed breast cancer cells (MCF7 and HCC1937) compared to the immortalized normal epithelial cell line MCF10. By modulating mitogenic pathways, we established a correlation between H1 tyrosine phosphorylation and cell proliferative status, enforcing the notion of a role of phosphorylated histones in the definition of the tumor phenotype. We give evidence that EGF treatment was able to induce a significant increase of tyrosine phosphorylation in H1, much more evident in MCF7 cells than in MCF10 cells. Next, we analyzed the effects that modulation of three signaling pathways, known to be altered in cancerogenesis, PI3K, PPAR γ and FAK, could have on phosphorylation in H1.

Phosphoinositide 3-kinase (PI3K) and its downstream mediator AKT are activated in many types of cancer and regulate many processes including proliferation, migration, apoptosis, differentiation and cell adhesion [21, 22]. Our data disclosed that the treatment with LY294002, a PI3K inhibitor, leads to a 50% reduction of tyrosine phosphorylation in H1 in both tumor cell types, suggesting that the kinase regulating this phosphorylation must be a downstream effector of PI3K signaling.

Furthermore, we treated tumor cells with Troglitazone, a PPAR γ agonist whose anti-tumor properties in breast cancer have been extensively reported [23]. Troglitazone belongs to Thiazolidinediones (TZDs) antidiabetic drugs and has antiproliferative effects [24] by both receptor dependent and independent actions. Peroxisome proliferator-activated receptor γ (PPAR γ) is a member of nuclear ligand-dependent transcription factor whose activation leads to growth inhibition in human breast cancer cells. Activation of PPAR γ controls cell migration by upregulating the expression of PTEN, that leads, in turn, to a decrease of FAK and paxillin phosphorylation [25]. In our study, treatment with Troglitazone induces a significant reduction of tyrosine phosphorylation levels on histone H1.

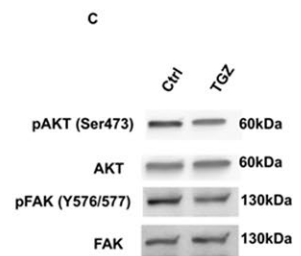
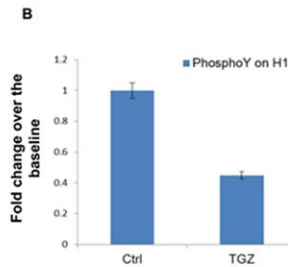
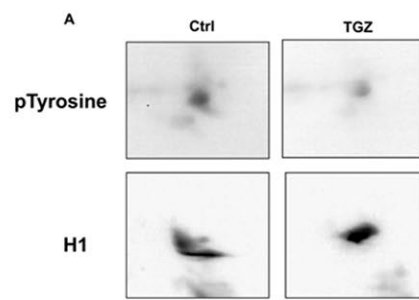
Panel A: LY294002 treatment

HCC1937



Panel B: Troglitazone treatment

HCC1937



Panel C: PND1186

HCC1937

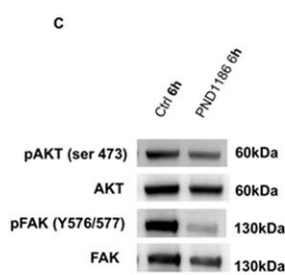
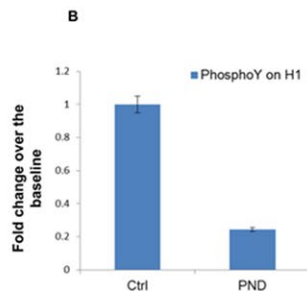
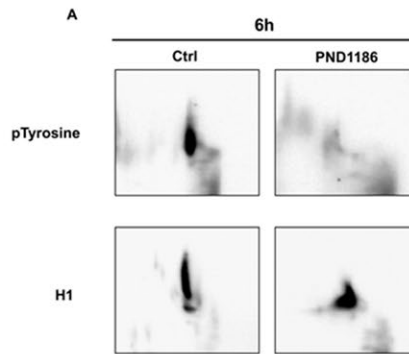


Figure 9. Analysis of H1 histone tyrosine phosphorylation following LY294002, Troglitazone and PND1186 treatments in HCC1937 cells. (A) Analysis of H1 histone tyrosine phosphorylation following LY294002 treatments in HCC1937 cells. (A) 2D TAU Western blot analysis of histone H1 tyrosine phosphorylation level (upper panel) and relative normalization with H1 antibody (lower panel) after treatment of HCC1937 with LY294002; All WB 2D images were acquired in 4 seconds. (B) Densitometry analysis of H1 tyrosine

phosphorylation spots; (C) Western blot analysis of pAKT, and pFAK (Y576/577) levels in protein extracts from LY294002 treated cells. Phospho-Akt (ser473) and pFAK (Y576/577) signals were normalized to the corresponding total Akt and total FAK respectively. (Panel B) Analysis of H1 histone tyrosine phosphorylation following Troglitazone treatments in HCC1937 cells. (A) 2D TAU Western blot analysis of histone H1 tyrosine phosphorylation level (upper panel) and relative normalization with H1 antibody (lower panel) after treatment of HCC1937 with Troglitazone; All WB 2D images were acquired in 4 seconds. (B) Densitometry analysis of H1 tyrosine phosphorylation spots; (C) Western blot analysis of pAKT, and pFAK (Y576/577) levels in protein extract from Troglitazone treated cells. Phospho-Akt (S473) and p-FAK (Y576/577) signals were normalized to the corresponding total Akt and total FAK respectively. (Panel C) Analysis of H1 histone tyrosine phosphorylation following PND1186 treatments in HCC1937 cells. (A) 2D TAU Western blot map of histone H1 tyrosine phosphorylation (upper panel) and relative normalization with H1 antibody (lower panel) after PND1186 treatment; All WB 2D images were acquired in 4 seconds. (B) Densitometry analysis of H1 tyrosine phosphorylation spots; (C) Western blot analysis of pAKT, and p-FAK levels in protein extract from PND1186 treated cells. Phospho-Akt (S473) and pFAK (Y576/577) signals were normalized to the corresponding total Akt and total FAK respectively. The assays were repeated in three independent biological replicates. Data are expressed as mean \pm SEM (N =3).

These results, together with the search of phosphorylation consensus, allowed us to focus the attention on Focal adhesion kinase (FAK), as a candidate for the H1 tyrosine phosphorylation. FAK is an evolutionarily conserved non-receptor tyrosine kinase that plays important roles in specific cellular functions such as adhesion, migration, invasion, polarity, proliferation and survival [26, 27]. The auto-phosphorylation of FAK at Y397 is the first step for its activation and creates a binding site for Src. Thus, Src phosphorylates several sites of FAK, including the

tyrosine 576 and 577 within the central kinase domain and positively regulates FAK kinase activity. AKT associates with FAK and directly modulates its expression through phosphorylation at several serine and threonine residues [31]. FAK is overexpressed in several cancers; specifically, high levels of FAK were found in breast cancer tissues and correlate with cancer progression and lymph node positivity [26]. Under normal conditions, FAK is typically a cytoplasmic kinase, but it can shuttle into the nucleus under appropriate stimuli in several cell

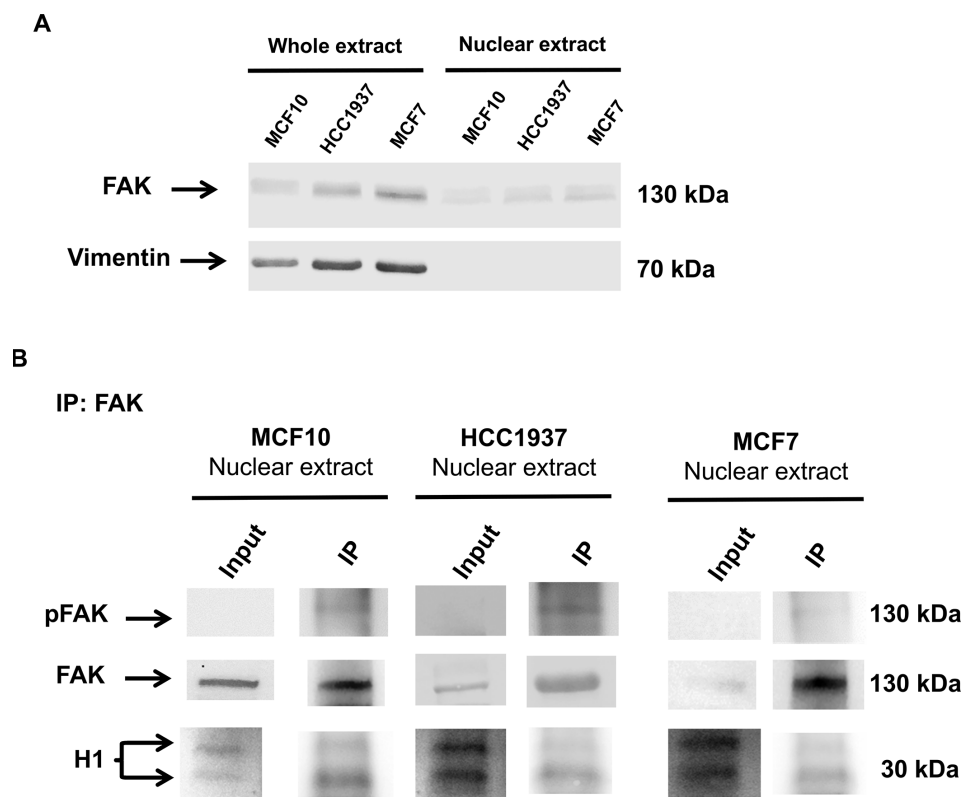


Figure 10. Immunoprecipitation analysis of nuclear FAK and histone H1. Immunoprecipitation (IP) analysis demonstrated that nuclear FAK associates with H1 histone. IP was carried out with anti-FAK antibody (3285, Cell signaling), followed by immunoblotting with anti-FAK (D2R2E, Cell signaling), anti-pFAK (Y576/577) and anti-H1 antibodies. IP experiments were done on MCF7, HCC1937 and MCF10 cell lines. The images are representative of three independent biological replicates. Panel A shows the levels of FAK in whole and nuclear extracts; Vimentin blot assess that nuclear extracts are not contaminated by cytoplasmic fraction.

types [28–32]. In the nuclei, FAK promotes p53 ubiquitination, acting as a scaffold [33]. Moreover, FAK has a role in histone PTMs promoting H3K27me3 through the regulation of zeste homolog 2 enhancer (EZH2) [34]. Nuclear FAK is associated with chromatin in squamous cell carcinoma (SCC) and interacts with a number of transcription factors and regulators [35, 36], interfering with GATA4 transcription factor and controlling chromatin structure [28].

Treatment with PND1186, a selective FAK inhibitor, induces in our cell systems a significant reduction of H1 tyrosine phosphorylation, detectable very early, as expected if FAK directly acts on the substrate.

The ability of FAK to directly interact with the histone H1 was supported by their co-immunoprecipitation, and co-localization during the interphase of cell cycle assessed immunofluorescence analysis.

In conclusion, this work offers a robust method for a comprehensive cover of PTMs occurring in histones in normal, sporadic and hereditary breast cancer cell lines. It proposes H1 tyrosine phosphorylation as novel PTM with a potential, relevant role in breast tumorigenesis and it candidates FAK as the kinase probably involved in H1 phosphorylation suggesting a novel key role of FAK in controlling post-translational events relevant in breast cancer proliferation.

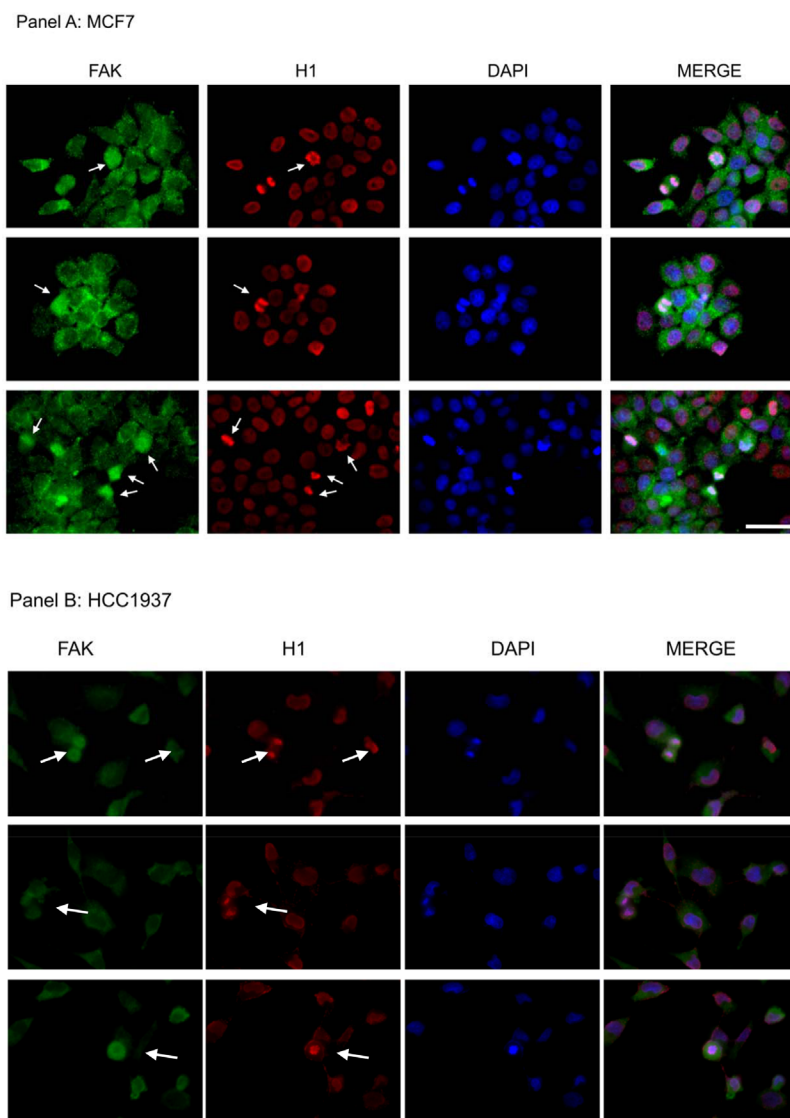


Figure 11. Assessment of FAK and H1 localization in MCF7 and HCC1937 cell lines. Immunofluorescence analysis of an asynchronous MCF7 cell population stained with antibodies against FAK (green) and H1 (red). Images of the cells captured at different stages of mitosis revealed FAK co-localization with H1 (white arrows). The nuclei were counterstained with DAPI (blue) and merge is also shown. Scale bar: 50 μ m. The images are representative of three independent biological replicates.

MATERIALS AND METHODS

Cell cultures

Human breast cancer cell line MCF7 (ATCC, Manassas, USA) was grown in Dulbecco's modified Eagle's medium (DMEM) (Sigma Aldrich, Saint Louis, Missouri, USA) supplemented with 10% (w/v) fetal bovine serum (FBS) (Sigma Aldrich), 100 mg/ml streptomycin and 100U/ml penicillin (Sigma Aldrich). MCF10 mammary epithelial cell line (ATCC, Manassas, USA) was grown in MEGM Mammary Epithelial Cell Growth Medium (Lonza, Walkersville, MD) supplemented with 20 ng/ml epidermal growth factor (Lonza), 0,5 µg/ml hydrocortisone (Lonza), 100 ng/ml cholera toxin (Sigma Aldrich) and 10 µg/ml insulin (Lonza). HCC1937 cell line was homozygous for the BRCA1 5382C mutation and was used as a model of hereditary breast cancer. They carried a mutation on TP53 gene with wild-type allele loss and a homozygous deletion of PTEN gene. HCC1937 cells (ATCC) were grown in RPMI medium (ATCC) supplemented with 20% (w/v) fetal bovine serum (FBS) (Sigma Aldrich), 100 mg/ml streptomycin and 100U/ml penicillin (Sigma Aldrich). The rate of cell in each cell cycle was assessed by FACS analysis. Histones used for the matching, were extracted from cell lines having a comparable distribution among the cell cycle phases.

Cell cycle was analyzed by propidium iodide (PI) staining and flow cytometry. Briefly, 1×10^6 cell, were fixed by resuspension in 500 µl of cold 70% ethanol under continuous gentle vortexing and left at 4°C 30 minutes or kept overnight at -20°C. Cells were then recovered by centrifugation, washed twice in PBS and incubated for 1h at room temperature in 1 ml PBS containing propidium iodide (20 µg/ml), NP40 0.1% and ribonuclease (40 µ/ml). Samples were analyzed by a BD™ LSRFortessa™ X-20 Flow Cytometer with 488-nm excitation and a 610/20nm bandpass emission filter. FlowJo™ software was used for data analysis.

Protein extraction

Histones extraction from mammalian cell culture

Acid-extraction of histone proteins was performed according to the protocol of Shechter et al. [9]. Cells were centrifuged at 1000xg for 5 min and resuspended in hypotonic lysis buffer (10 mM Tris-Cl pH 8.0, 1 mM KCl, 1.5 mM MgCl₂, 1 mM DTT, 1 mM phenyl-methylsulfonyl fluoride, PMSF) supplemented with protease and phosphatase inhibitor cocktail (Halt Protease Inhibitor Cocktail/ Halt Phosphatase Inhibitor Cocktail, Thermo Fisher Scientific Inc.) at a density of 5×10^6 cells ml⁻¹. Cells lysate was

incubated for 30 min on rotator at 4°C. Nuclei were isolated by centrifugation at 10000 ×g for 10 min at 4°C. Histones were extracted by incubation with 0.4 N H₂SO₄ on ice. Proteins were precipitated using trichloroacetic acid (TCA). Histone pellets were washed twice with ice-cold acetone, lyophilized and then solubilized in sterile H₂O. The extraction was verified by 1D-TAU GEL. Resulting gel was stained with EZBlue Gel Staining Reagent (Sigma Aldrich).

Whole protein extraction

Cells lines were washed with PBS and lysed at 0°C for 30 min using lysis buffer (15 mM Tris pH7.5, 120mM NaCl, 25mM KCl, 0.5% Triton X-100, supplemented with protease and phosphatase inhibitor cocktail). Cell lysate was sonicated at 4 °C for 10 sec and subsequently centrifuged at 15000× g for 20 min. Supernatant was carefully removed and protein content was measured by the Bradford method (BioRad, Hercules, CA) [37]; and the supernatants were stored at 80°C.

Isolation of nuclear and cytosolic fractions

Cells were collected with 1ml of hypotonic lysis buffer (10 mM Tris-Cl pH 8.0, 1 mM KCl, 1.5 mM MgCl₂, 1 mM DTT, supplemented with protease and phosphatase inhibitor cocktail) and incubated for 30 min on rotator at 4°C. Cell lysate was centrifuged at 10000×g for 10 min at 4°C to isolate nuclei [38, 39]. Cytosol was supplemented with 1% Triton X-100. Both fractions were incubated on ice for 30 minutes and then centrifuged at 15000xg for 20 min at 4°C. Protein concentration was determined using the Bradford Protein Assay (Bio-Rad) according to the manufacturer's instructions with BSA as standards.

2D gel electrophoresis

First dimension: triton-acid-urea (TAU) gel electrophoresis

TAU gel was prepared according to the protocol of Shechter et al. [11]. Thirty-five µg of lyophilized histone powder was dissolved in acidic sample buffer (6 M Urea, 5% glacial acetic acid, 0.02% Pyronin Y) and loaded on the gel. The gel was run in 5% acetic acid solution at the voltage of 25 V for about 17h. The gel was then stained with EZBlue Gel Staining Reagent (Sigma Aldrich) to evaluate proteins separation.

Second dimension: SDS-PAGE gel electrophoresis

Lanes of TAU gel, containing resolved histones, were cut and transferred to the top of a 12% SDS polyacrylamide gels (Mini-PROTEAN® TGX™ Precast Gels, IPG Well) for the separation based on molecular weight. Second dimension was run at 80 V until the bromophenol blue dye front reached the end of the gels [12]. Gels were stained with EZBlue Gel Staining Reagent (Sigma

Aldrich) or MS compatible silver staining procedure. The analysis was performed in triplicate. Gel image analysis was carried out using the Image Master 2D-Platinum software 6.0 (GE Healthcare) [40, 41].

In-gel tryptic digestion

Protein spots, obtained from 2D TAU/SDS gels, were manually excised, destained, and dehydrated in acetonitrile. They were then rehydrated and digested in trypsin solution by overnight incubation at 37°C. After drying the organic solvent, the tryptic peptides were purified by Pierce C18 Spin Columns (Thermo Fisher Scientific Inc.) for desalting before mass spectrometric analysis. The purified peptides were eluted with 40µL of 70% acetonitrile and dehydrated in a vacuum evaporator [42, 43].

Nanoscale LC-MS/MS analysis

LC-MS/MS analysis was performed using an Easy LC 1000 nanoscale liquid chromatography (nanoLC) system (Thermo Fisher Scientific, Odense, Denmark). The analytical nanoLC column was a pulled fused silica capillary, 75 µm i.d., in-house packed to a length of 10 cm with 3 µm C18 silica particles from Dr. Maisch (Entringen, Germany). The peptide mixtures were loaded at 500 nL/min directly onto the analytical column. A binary gradient was used for peptide elution. Mobile phase A was 0.1% formic acid, 2% acetonitrile, whereas mobile phase B was 0.1% formic acid, 80% acetonitrile. Gradient elution was achieved at 350 nL/min flow rate, and ramped from 0% B to 30% B in 15 minutes, and from 30% B to 100% B in additional 5 minutes; after 5 minutes at 100% B, the column was re-equilibrated at 0% B for 10 minutes before the following injection. MS detection was performed on a quadrupole-orbitrap mass spectrometer Q-Exactive (Thermo Fisher Scientific, Bremen, Germany) operating in positive ion mode, with nanoelectrospray (nESI) potential at 1800 V applied on the column front-end via a tee piece. Data-dependent acquisition was performed by using a top-4 method with resolution (FWHM), AGC target and maximum injection time (ms) for full MS and MS/MS of, respectively, 70,000/17,500, 1e6/5e5, 50/400. Mass window for precursor ion isolation was 2.0 m/z, whereas normalized collision energy was 30. Ion threshold for triggering MS/MS events was 2e4. Dynamic exclusion was 15 s [43, 44].

MS data processing and database searching

The acquired raw data files were preprocessed with Proteome Discoverer 1.4 (Thermo Fisher Scientific, Bremen, Germany). MS/MS data were searched on the

Human UniProt database. False discovery rate (FDR) of peptide identifications was estimated using the “Target-decoy PSM validator” node in Proteome Discoverer [45]. The following search parameters were used: MS error tolerance: 5 ppm; MS/MS error tolerance: 0.02 Da; enzyme specificity: trypsin; maximum number of missed cleavages: 2; taxonomy Human; fixed modifications: Carbamidomethylation (C); variable modification: Oxidation (M), Acetyl (K), Methyl (K), Dimethyl (K), Trimethyl (K), Methyl (R), Dimethyl (R), Deamidated (R) and Phosphorylation (STY). Protein hits based on two successful peptide identifications ($X_{corr} > 2.0$ for doubly charged peptides, >2.5 for triply charged peptides, and >3.0 for peptides having a charge state >3) were considered valid. All the MS/MS spectra, referred to modified peptides, were carefully verified by manually validation.

Western blot analyses

For 1D Western blot analysis, five µg of each histone sample was resolved by 15% SDS-PAGE and electro-transferred to a nitrocellulose membrane with a Trans-blots turbo system (Biorad). Membranes were incubated using the following primary antibodies: H4K16ac (1:1000; Cell signaling E2B8W), H4K20me3 (1:1000; Cell signaling D84D2), H3K9ac (1:1000; Cell signaling C5B11), H3K9me2-3 (1:1000; Cell signaling 6F12) and H3K18ac (1:1000; Cell signaling D8Z5H). Only for SirT1 analysis, fifty µg of total cells proteins extract were loaded in a 4–20% SDS-PAGE (Biorad), transferred to a membrane and blotted with the SirT1 antibody (1:1000; Cell signaling 1F3). To ensure equal loading of proteins was used a goat polyclonal anti- γ -Tubulin antibody (C-20) (1:1000; sc-7396, Santa Cruz Biotechnology).

For 2D Western blot analysis, equal amounts of histone extracts were resolved by 2D TAU/SDS gel. To minimize gel to gel variation and ensure a reliable comparison among analyzed samples second dimension for each sample was run on Mini-PROTEAN® TGX™ Precast Gels, IPG Well (12%). Resulting gel were transferred to nitrocellulose membranes with a Trans-blots turbo system (Biorad) using Trans-Blot® Turbo™ Mini Nitrocellulose Transfer Packs. Membranes were probed using the Phospho-Tyrosine (1:2000; Cell signaling P-Tyr-100) antibody. Phospho-Tyrosine signals were normalized to the corresponding total H1 (1:1000; Abcam ab71594).

To ensure equal protein loading, membranes were incubated with red ponceau solution (P7170 Sigma-Aldrich). Images were acquired using Image scanner II (GE Healthcare). Membrane image were visualized using image master 2D platinum.

Cell treatments

Cells at 50% confluence were serum starved for 24 h. Cell treatments were performed using recombinant human EGF (PeproTech) C_f: 50ng/ml, LY294002 (Sigma Aldrich) C_f: 30μM, Troglitazone (MedChemExpress) C_f: 50μM and PND1186 (MedChemExpress) C_f: 300nM.

Flow cytometry experiment was done to assess the rate of cell cycle phases after treatment, cells were collected, fixed with 70% ethanol, stained with propidium iodide solution and analyzed by flow cytometry.

Histone pattern was analyzed by 2D TAU Western blot using Phospho-Tyrosine (1:2000; Cell signaling P-Tyr-100) and H1 (1:100; Abcam ab71594) antibodies.

Whole proteins extract and nuclear protein fraction were analyzed by Western blotting using the following primary antibodies: pAKT (Ser473) (1:1000; D9E), AKT (1:1000; 9272), pFAK (Tyr397) (1:200; D20B1), pFAK (Tyr576/577) (1:500) and FAK (1:1000; all Cell signaling).

Densitometric analysis

Secondary antibodies signal was revealed by Pierce ECL Western Blotting Substrate (Thermo scientific). Images were acquired using the UViSoft Image quantification software. Signals intensities were assessed by densitometry using the Alliance 4.7 software. For each 2D western blot the exposure times were fixed to 10 seconds for phosphotyrosine signal detection and 5 seconds for total histone H1 signal detection.

Densitometric analysis of 2D Western Blotting spots was performed by Image Master 2D- Platinum software 6.0 (GE Healthcare). Data were analyzed using Excel spreadsheet (Microsoft office), and expressed as mean ± SEM (N =3), where SEM represents the standard error of the mean and N indicates the number of experimental repeats. Statistical analysis was performed using one-way ANOVA, followed by Dunnett's multiple comparisons test. Differences were considered significant when P ≤ 0.05.

Cell proliferation assay

CellTrace™ CFSE Cell Proliferation assay has been performed in accordance with manufacturer instruction. Cell labeling was carried out as follows. CellTrace™ DMSO stock solution was diluted in phosphate-buffered saline (PBS) at the working concentration of 5μM. Cell pellet was obtained by centrifugation and cells were gently resuspended in prewarmed (37°C) PBS containing the dye and incubated for 20 minutes at

room temperature protected from light. Cells were then washed twice with five times the original staining volume by culture medium containing FCS to remove any free dye remaining in the solution. Cells were finally plated in fresh, pre-warmed complete culture medium, analyzed, treated and cultured as indicated. FACS analysis was performed using a BD™ LSRFortessa™ X20 Flow Cytometer with 488-nm excitation and a 530/30-nm bandpass emission filter. Data were analyzed and proliferation index, defined as the total number of divisions divided by the number of cells that went into division, was generated, by ModFit LT™ 4.0 software.

Immunoprecipitation analysis

Four hundred μg of nuclear protein extracts from untreated cells was subjected to immunoprecipitation with FAK antibody (Cell signaling, 3285). After overnight incubation at 4°C, protein A/G PLUS-Agarose beads (Santa Cruz Biotechnology) were added to the mixture and incubated for 4h at 4°C. Beads were washed three times and boiled for 5 minutes. Immunocomplexes were resolved on 4-20% SDS gel, blotted using a Trans-blot turbo system (Biorad) for 30 minutes at 30V, 1.0A and then subjected to immunoblot analysis using the following antibodies: pFAK (Tyr397) (1:200; D20B1), FAK (D2R2E, Cell signaling)(1:1000) and H1 (1:100; Abcam ab71594).

The assays were repeated in three independent biological replicates. Whole and nuclear extract (100 μg each) were resolved by pre cast SDS-PAGE (Any kD™ Mini-PROTEAN Precast Protein Gels, Biorad) and electrotransferred to a nitrocellulose membrane with a Trans-blot turbo system (Biorad). Membranes were incubated using the following primary antibodies: FAK (D2R2E, Cell signaling)(1:1000), Vimentin (5741, Cell signaling, 1:1000). The detection of a primary antibody was done with antirabbit horseradish peroxidase-conjugate secondary antibodies (Cell Signaling). Blots were developed using the SuperSignal West Femto ECL substrate (Pierce, Thermo Fisher Scientific Inc., Bremen, Germany). Images were acquired using Alliance 2.7 (UVITEC, Eppendorf, Milan, Italy)

Immunofluorescence

Cells were fixed with 4% paraformaldehyde (Sigma-Aldrich) for 30 min. After permeabilization with 0.3% Triton X-100 (Sigma-Aldrich) in phosphate buffered saline (PBS) for 15 min, the cells were blocked with 10% FBS (Biowest) and 0.1% Triton X-100 in PBS for 1 h at room temperature and then incubated with H1 (1:100, Abcam ab71594) and FAK (1:100, Cell Signaling, 3285) primary antibodies diluted in PBS

containing 3% FBS. Goat anti-mouse Alexa-Fluor-647 (A-21235, Life Technologies) and goat anti-rabbit Alexa-Fluor-488 (A-11008, Life Technologies) were used as the secondary antibodies at a concentration of 2 µg/ml in PBS containing 1% FBS for 45 min at room temperature. Nuclei were stained with DAPI (4',6-diamidino-2-phenylindole). Slides were mounted with fluorescent mounting medium (Dako Cytomation) and images were acquired with DMi8 Leica microscope. The assays were repeated in three independent biological replicates

AUTHOR CONTRIBUTIONS

DS and GC conceived and designed the experiments; AMP performed gel TAU experiments and proteomics analysis. MTDA performed immunofluorescence analysis. EO, AC, LT and CVF performed western blot and immunoprecipitation experiments; VA supervised in vitro experiments on cell lines and critically revised the manuscript. DS, VA and GC wrote the paper.

CONFLICTS OF INTEREST

The authors declare no conflict of interest." The founding sponsors had no role in the design of the study; in the collection, analyses, or interpretation of data; in the writing of the manuscript, and in the decision to publish the results.

FUNDING

This work was supported in part by the MIUR grant PON03PE_00009_2 (iCARE) to GC and by internal grant from Department of experimental and clinical medicine (UMG) to DS. AMP was supported by fellowships from the PhD Programme in Medical Biotechnology. EO was supported by fellowships from the PhD Programme in Molecular and translational oncology and innovative medical surgical technologies; AC was supported by fellowships from the PhD Programme in Molecular and translational oncology and innovative medical surgical technologies; CVF was supported by fellowships from the PhD Programme in Molecular and translational oncology and innovative medical surgical technologies.

REFERENCES

1. Rothbart SB, Strahl BD. Interpreting the language of histone and DNA modifications. *Biochim Biophys Acta*. 2014; 1839:627–43. <https://doi.org/10.1016/j.bbagr.2014.03.001> PMID:24631868
2. Kornberg RD, Lorch Y. Twenty-five years of the nucleosome, fundamental particle of the eukaryote chromosome. *Cell*. 1999; 98:285–94. [https://doi.org/10.1016/S0092-8674\(00\)81958-3](https://doi.org/10.1016/S0092-8674(00)81958-3) PMID:10458604
3. Khan SA, Reddy D, Gupta S. Global histone post-translational modifications and cancer: biomarkers for diagnosis, prognosis and treatment? *World J Biol Chem*. 2015; 6:333–45. <https://doi.org/10.4331/wjbc.v6.i4.333> PMID:26629316
4. Hergeth SP, Schneider R. The H1 linker histones: multifunctional proteins beyond the nucleosomal core particle. *EMBO Rep*. 2015; 16:1439–53. <https://doi.org/10.15252/embr.201540749> PMID:26474902
5. Byler S, Goldgar S, Heerboth S, Leary M, Housman G, Moulton K, Sarkar S. Genetic and epigenetic aspects of breast cancer progression and therapy. *Anticancer Res*. 2014; 34:1071–77. PMID:24596345
6. Portela A, Esteller M. Epigenetic modifications and human disease. *Nat Biotechnol*. 2010; 28:1057–68. <https://doi.org/10.1038/nbt.1685> PMID:20944598
7. Fraga MF, Ballestar E, Villar-Garea A, Boix-Chornet M, Espada J, Schotta G, Bonaldi T, Haydon C, Ropero S, Petrie K, Iyer NG, Pérez-Rosado A, Calvo E, et al. Loss of acetylation at Lys16 and trimethylation at Lys20 of histone H4 is a common hallmark of human cancer. *Nat Genet*. 2005; 37:391–400. <https://doi.org/10.1038/ng1531> PMID:15765097
8. Rodríguez-Paredes M, Esteller M. Cancer epigenetics reaches mainstream oncology. *Nat Med*. 2011; 17:330–39. <https://doi.org/10.1038/nm.2305> PMID:21386836
9. Elsheikh SE, Green AR, Rakha EA, Powe DG, Ahmed RA, Collins HM, Soria D, Garibaldi JM, Paish CE, Ammar AA, Grainge MJ, Ball GR, Abdelghany MK, et al. Global histone modifications in breast cancer correlate with tumor phenotypes, prognostic factors, and patient outcome. *Cancer Res*. 2009; 69:3802–09. <https://doi.org/10.1158/0008-5472.CAN-08-3907> PMID:19366799
10. Yokoyama Y, Matsumoto A, Hieda M, Shinchi Y, Ogihara E, Hamada M, Nishioka Y, Kimura H, Yoshidome K, Tsujimoto M, Matsuura N. Loss of histone H4K20 trimethylation predicts poor prognosis in breast cancer and is associated with invasive activity. *Breast Cancer Res*. 2014; 16:R66. <https://doi.org/10.1186/bcr3681> PMID:24953066
11. Shechter D, Dormann HL, Allis CD, Hake SB. Extraction, purification and analysis of histones. *Nat Protoc*. 2007; 2:1445–57. <https://doi.org/10.1038/nprot.2007.202> PMID:17545981

12. Zhang W, Tang X, Ding M, Zhong H. Cu²⁺-assisted two dimensional charge-mass double focusing gel electrophoresis and mass spectrometric analysis of histone variants. *Anal Chim Acta*. 2014; 852:121–28. <https://doi.org/10.1016/j.aca.2014.08.038> PMID:25441888
13. Kan PY, Caterino TL, Hayes JJ. The H4 tail domain participates in intra- and internucleosome interactions with protein and DNA during folding and oligomerization of nucleosome arrays. *Mol Cell Biol*. 2009; 29:538–46. <https://doi.org/10.1128/MCB.01343-08> PMID:19001093
14. Scumaci D, Tammè L, Fiumara CV, Pappaianni G, Concolino A, Leone E, Faniello MC, Quaresima B, Ricevuto E, Costanzo FS, Cuda G. Plasma Proteomic Profiling in Hereditary Breast Cancer Reveals a BRCA1-Specific Signature: Diagnostic and Functional Implications. *PLoS One*. 2015; 10:e0129762. <https://doi.org/10.1371/journal.pone.0129762> PMID:26061043
15. Michalak EM, Visvader JE. Dysregulation of histone methyltransferases in breast cancer - Opportunities for new targeted therapies? *Mol Oncol*. 2016; 10:1497–515. <https://doi.org/10.1016/j.molonc.2016.09.003> PMID:27717710
16. Shinkai Y, Tachibana M. H3K9 methyltransferase G9a and the related molecule GLP. *Genes Dev*. 2011; 25:781–88. <https://doi.org/10.1101/gad.2027411> PMID:21498567
17. Tachibana M, Sugimoto K, Nozaki M, Ueda J, Ohta T, Ohki M, Fukuda M, Takeda N, Niida H, Kato H, Shinkai Y. G9a histone methyltransferase plays a dominant role in euchromatic histone H3 lysine 9 methylation and is essential for early embryogenesis. *Genes Dev*. 2002; 16:1779–91. <https://doi.org/10.1101/gad.989402> PMID:12130538
18. Rifai K, Judes G, Idrissou M, Daures M, Bignon YJ, Penault-Llorca F, Bernard-Gallon D. SIRT1-dependent epigenetic regulation of H3 and H4 histone acetylation in human breast cancer. *Oncotarget*. 2018; 9:30661–78. <https://doi.org/10.18632/oncotarget.25771> PMID:30093977
19. Kuzmichev A, Margueron R, Vaquero A, Preissner TS, Scher M, Kirmizis A, Ouyang X, Brockdorff N, Abate-Shen C, Farnham P, Reinberg D. Composition and histone substrates of polycomb repressive group complexes change during cellular differentiation. *Proc Natl Acad Sci USA*. 2005; 102:1859–64. <https://doi.org/10.1073/pnas.0409875102> PMID:15684044
20. Rikova K, Guo A, Zeng Q, Possemato A, Yu J, Haack H, Nardone J, Lee K, Reeves C, Li Y, Hu Y, Tan Z, Stokes M, et al. Global survey of phosphotyrosine signaling identifies oncogenic kinases in lung cancer. *Cell*. 2007; 131:1190–203. <https://doi.org/10.1016/j.cell.2007.11.025> PMID:18083107
21. Wang YA, Johnson SK, Brown BL, McCarragher LM, Al-Sakkaf K, Royds JA, Dobson PR. Enhanced anti-cancer effect of a phosphatidylinositol-3 kinase inhibitor and doxorubicin on human breast epithelial cell lines with different p53 and oestrogen receptor status. *Int J Cancer*. 2008; 123:1536–44. <https://doi.org/10.1002/ijc.23671> PMID:18634052
22. Lien EC, Dibble CC, Toker A. PI3K signaling in cancer: beyond AKT. *Curr Opin Cell Biol*. 2017; 45:62–71. <https://doi.org/10.1016/j.ceb.2017.02.007> PMID:28343126
23. Yu HN, Lee YR, Noh EM, Lee KS, Kim JS, Song EK, Han MK, Lee YC, Kwon KB, Lee SJ, Youn HJ, Jung SH. Induction of G1 phase arrest and apoptosis in MDA-MB-231 breast cancer cells by troglitazone, a synthetic peroxisome proliferator-activated receptor gamma (PPARgamma) ligand. *Cell Biol Int*. 2008; 32:906–12. <https://doi.org/10.1016/j.cellbi.2008.04.011> PMID:18474441
24. Han S, Roman J. Peroxisome proliferator-activated receptor gamma: a novel target for cancer therapeutics? *Anticancer Drugs*. 2007; 18:237–44. <https://doi.org/10.1097/CAD.0b013e328011e67d> PMID:17264754
25. Chen Y, Wang SM, Wu JC, Huang SH. Effects of PPARgamma agonists on cell survival and focal adhesions in a Chinese thyroid carcinoma cell line. *J Cell Biochem*. 2006; 98:1021–35. <https://doi.org/10.1002/jcb.20839> PMID:16795079
26. Chatzizacharias NA, Kouraklis GP, Theocharis SE. Clinical significance of FAK expression in human neoplasia. *Histol Histopathol*. 2008; 23:629–50. PMID:18283648
27. Serrels A, Lund T, Serrels B, Byron A, McPherson RC, von Kriegsheim A, Gómez-Cuadrado L, Canel M, Muir M, Ring JE, Maniati E, Sims AH, Pachter JA, et al. Nuclear FAK controls chemokine transcription, Tregs, and evasion of anti-tumor immunity. *Cell*. 2015; 163:160–73. <https://doi.org/10.1016/j.cell.2015.09.001> PMID:26406376
28. Kleinschmidt EG, Schlaepfer DD. Focal adhesion kinase signaling in unexpected places. *Curr Opin Cell Biol*. 2017; 45:24–30.

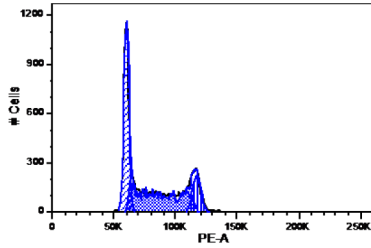
- <https://doi.org/10.1016/j.ceb.2017.01.003>
PMID:[28213315](https://pubmed.ncbi.nlm.nih.gov/28213315/)
29. Walsh C, Tanjoni I, Uryu S, Tomar A, Nam JO, Luo H, Phillips A, Patel N, Kwok C, McMahon G, Stupack DG, Schlaepfer DD. Oral delivery of PND-1186 FAK inhibitor decreases tumor growth and spontaneous breast to lung metastasis in pre-clinical models. *Cancer Biol Ther.* 2010; 9:778–90.
<https://doi.org/10.4161/cbt.9.10.11433>
PMID:[20234193](https://pubmed.ncbi.nlm.nih.gov/20234193/)
30. Tanjoni I, Walsh C, Uryu S, Tomar A, Nam JO, Mielgo A, Lim ST, Liang C, Koenig M, Sun C, Patel N, Kwok C, McMahon G, et al. PND-1186 FAK inhibitor selectively promotes tumor cell apoptosis in three-dimensional environments. *Cancer Biol Ther.* 2010; 9:764–77.
<https://doi.org/10.4161/cbt.9.10.11434>
PMID:[20234191](https://pubmed.ncbi.nlm.nih.gov/20234191/)
31. Wang S, Basson MD. Protein kinase B/AKT and focal adhesion kinase: two close signaling partners in cancer. *Anticancer Agents Med Chem.* 2011; 11:993–1002.
<https://doi.org/10.2174/187152011797927661>
PMID:[22023045](https://pubmed.ncbi.nlm.nih.gov/22023045/)
32. Cardoso AC, Pereira AH, Ambrosio AL, Consonni SR, Rocha de Oliveira R, Bajgelman MC, Dias SM, Franchini KG. FAK Forms a Complex with MEF2 to Couple Biomechanical Signaling to Transcription in Cardiomyocytes. *Structure.* 2016; 24:1301–10.
<https://doi.org/10.1016/j.str.2016.06.003>
PMID:[27427476](https://pubmed.ncbi.nlm.nih.gov/27427476/)
33. Lim ST, Chen XL, Lim Y, Hanson DA, Vo TT, Howerton K, Larocque N, Fisher SJ, Schlaepfer DD, Ilic D. Nuclear FAK promotes cell proliferation and survival through FERM-enhanced p53 degradation. *Mol Cell.* 2008; 29:9–22. <https://doi.org/10.1016/j.molcel.2007.11.031>
PMID:[18206965](https://pubmed.ncbi.nlm.nih.gov/18206965/)
34. Gnani D, Romito I, Artuso S, Chierici M, De Stefanis C, Panera N, Crudele A, Ceccarelli S, Carcarino E, D’Oria V, Porru M, Giorda E, Ferrari K, et al. Focal adhesion kinase depletion reduces human hepatocellular carcinoma growth by repressing enhancer of zeste homolog 2. *Cell Death Differ.* 2017; 24:889–902.
<https://doi.org/10.1038/cdd.2017.34>
PMID:[28338656](https://pubmed.ncbi.nlm.nih.gov/28338656/)
35. Lim ST. Nuclear FAK: a new mode of gene regulation from cellular adhesions. *Mol Cells.* 2013; 36:1–6.
<https://doi.org/10.1007/s10059-013-0139-1>
PMID:[23686429](https://pubmed.ncbi.nlm.nih.gov/23686429/)
36. Morozevich GE, Kozlova NI, Ushakova NA, Preobrazhenskaya ME, Berman AE. Integrin $\alpha 5 \beta 1$ simultaneously controls EGFR-dependent proliferation and Akt-dependent pro-survival signaling in epidermoid carcinoma cells. *Aging (Albany NY).* 2012; 4:368–74.
<https://doi.org/10.18632/aging.100457>
PMID:[22626691](https://pubmed.ncbi.nlm.nih.gov/22626691/)
37. Bradford MM. A rapid and sensitive method for the quantitation of microgram quantities of protein utilizing the principle of protein-dye binding. *Anal Biochem.* 1976; 72:248–54.
[https://doi.org/10.1016/0003-2697\(76\)90527-3](https://doi.org/10.1016/0003-2697(76)90527-3)
PMID:[942051](https://pubmed.ncbi.nlm.nih.gov/942051/)
38. Cox MM, Doudna J, O’Donnell M. *Molecular Biology: Principles and Practice* ISBN -13: 978-1464126147 ISBN-10: 1464126143. Edition: 2nd.
39. Concolino A, Olivo E, Tammè L, Fiumara CV, De Angelis MT, Quaresima B, Agosti V, Costanzo FS, Cuda G, Scumaci D. Proteomics Analysis to Assess the Role of Mitochondria in BRCA1-Mediated Breast Tumorigenesis. *Proteomes.* 2018; 6:E16.
<https://doi.org/10.3390/proteomes6020016>
PMID:[29584711](https://pubmed.ncbi.nlm.nih.gov/29584711/)
40. Weiss W, Görg A. High-resolution two-dimensional electrophoresis. *Methods Mol Biol.* 2009; 564:13–32.
https://doi.org/10.1007/978-1-60761-157-8_2
PMID:[19544015](https://pubmed.ncbi.nlm.nih.gov/19544015/)
41. Seillier-Moisewitsch F. *The Proteomics Protocols Handbook.* 2005; 239–258.
<https://doi.org/10.1385/1-59259-890-0:239>
42. Sinha P, Poland J, Schnölzer M, Rabilloud T. A new silver staining apparatus and procedure for matrix-assisted laser desorption/ionization-time of flight analysis of proteins after two-dimensional electrophoresis. *Proteomics.* 2001; 1:835–40.
[https://doi.org/10.1002/1615-9861\(200107\)1:7<835::aid-prot835>3.0.co;2-2](https://doi.org/10.1002/1615-9861(200107)1:7<835::aid-prot835>3.0.co;2-2)
PMID:[11503208](https://pubmed.ncbi.nlm.nih.gov/11503208/)
43. Hellman U, Wernstedt C, Góñez J, Heldin CH. Improvement of an “In-Gel” digestion procedure for the micropreparation of internal protein fragments for amino acid sequencing. *Anal Biochem.* 1995; 224:451–55.
<https://doi.org/10.1006/abio.1995.1070>
PMID:[7710111](https://pubmed.ncbi.nlm.nih.gov/7710111/)
44. Rappsilber J, Ishihama Y, Mann M. Stop and go extraction tips for matrix-assisted laser desorption/ionization, nanoelectrospray, and LC/MS sample pretreatment in proteomics. *Anal Chem.* 2003; 75:663–70. <https://doi.org/10.1021/ac026117i>
PMID:[12585499](https://pubmed.ncbi.nlm.nih.gov/12585499/)
45. Gaspari M, Cuda G. Nano LC-MS/MS: a robust setup for proteomic analysis. *Methods Mol Biol.* 2011; 790:115–26.
https://doi.org/10.1007/978-1-61779-319-6_9
PMID:[21948410](https://pubmed.ncbi.nlm.nih.gov/21948410/)

46. Chen G, Du C, Shen Z, Peng L, Xie H, Zang R, Li H, Xia Y, Tang W. MicroRNA-939 inhibits cell proliferation via targeting LRSAM1 in Hirschsprung's disease. *Aging (Albany NY)*. 2017; 9:2471–79.

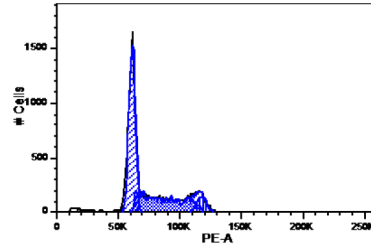
<https://doi.org/10.18632/aging.101331>

PMID:[29253842](https://pubmed.ncbi.nlm.nih.gov/29253842/)

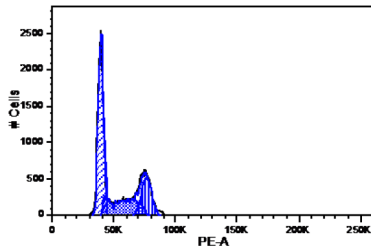
SUPPLEMENTARY MATERIALS



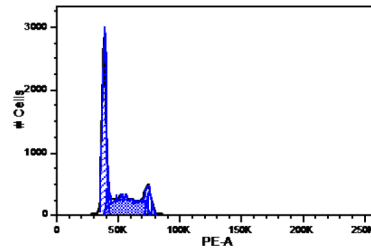
Watson Pragmatic: %G1 = 40.9; %S = 45.5; %G2 = 14.3.
Cell Cycle
MCF7_60%_001.fcs
Event Count: 14145



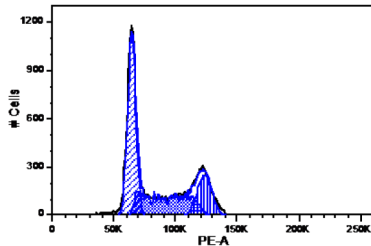
Watson Pragmatic: %G1 = 51.6; %S = 36.1; %G2 = 8.29.
Cell Cycle
MCF7_100%_002.fcs
Event Count: 18637



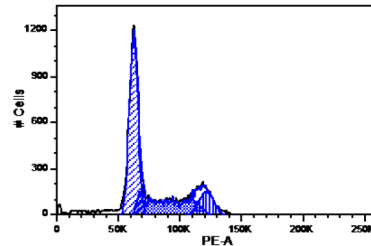
Watson Pragmatic: %G1 = 49.7; %S = 27.7; %G2 = 21.9.
Cell Cycle
MCF10_60%_003.fcs
Event Count: 25998



Watson Pragmatic: %G1 = 46.9; %S = 41.2; %G2 = 9.65.
Cell Cycle
MCF10_100%_004.fcs
Event Count: 23090

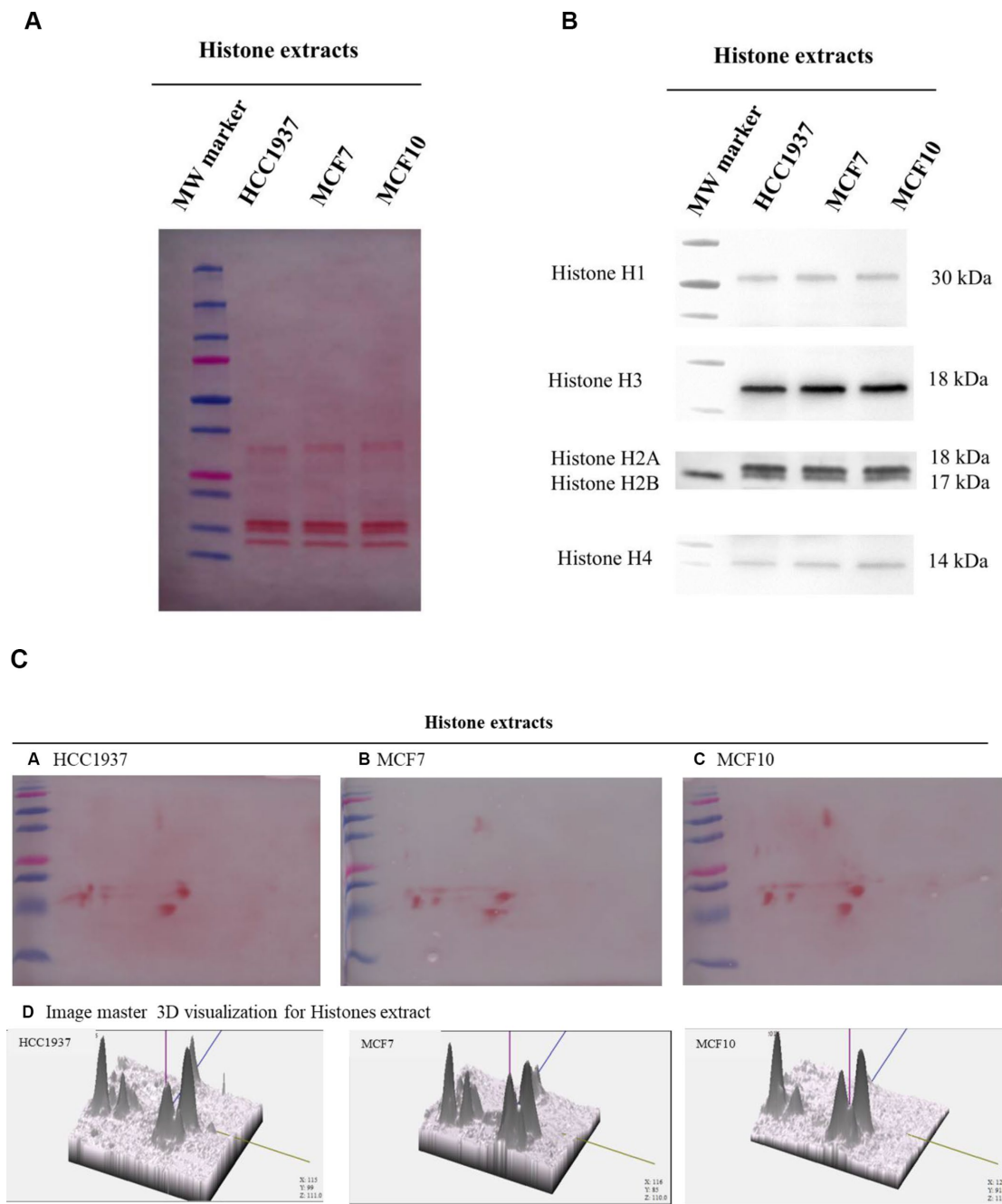


Watson Pragmatic: %G1 = 46.4; %S = 31.9; %G2 = 19.5.
Cell Cycle
HCC1937_60%_005.fcs
Event Count: 19561



Watson Pragmatic: %G1 = 53; %S = 28.4; %G2 = 12.6.
Cell Cycle
HCC1937_100%_006.fcs
Event Count: 19004

Supplementary Figure 1. Cell cycle analysis. 1×10^6 cell, were fixed by resuspension in 500 μ l of cold 70% ethanol under continuous gentle vortexing and incubated at 4°C 30 minutes or kept overnight at -20°C. Cells were then recovered by centrifugation, washed twice in PBS and incubated for 1h at room temperature in 1 ml PBS containing propidium iodide (20 μ g/ml), NP40 0.1% and ribonuclease (40 μ /ml). Samples were analysed by a BD™ LSRFortessa™ X-20 Flow Cytometer with 488-nm excitation and a 610/20nm bandpass emission filter. FlowJo™ software was used for data analysis.



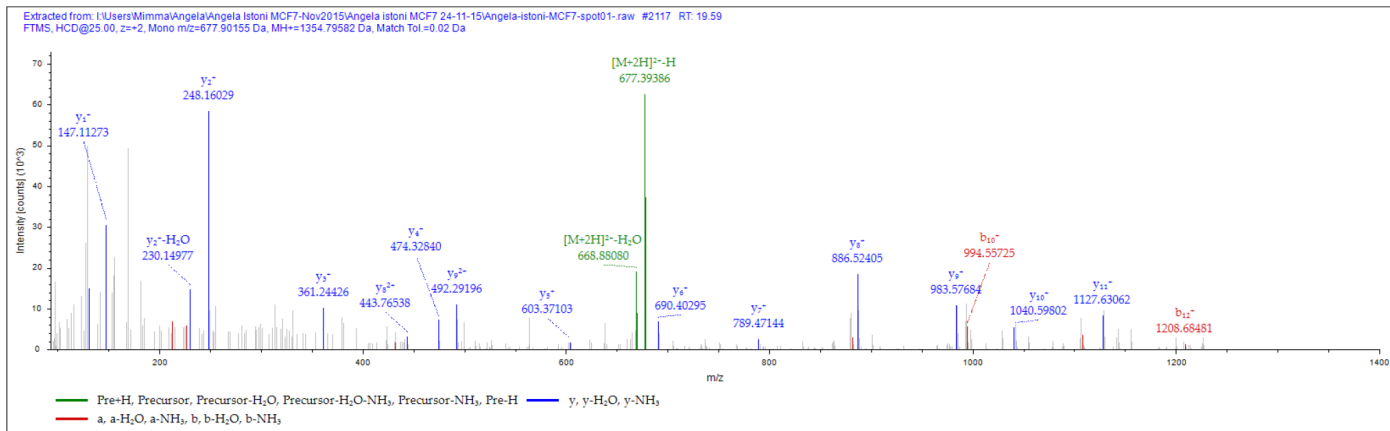
Supplementary Figure 2. Western blot detection of Histone proteins. (A) Red ponceau Staining of membrane. Histones extracts (5 micrograms) were resolved using 15% SDS-PAGE and electrotransferred to a nitrocellulose membrane with a Trans-blot turbo system (Biorad). Membranes were stained using red ponceau solution (P7170 Sigma-Aldrich). Nitrocellulose membrane was destained using PBS 1X and used for immunologically detection. (B) Immunoblotting. Membranes were incubated using the following primary antibodies: Histone H1 (1:1000; Abcam ab71594), Histone H2B (D2H6) (1:1000; Cell signaling 112364), Histone H2A (1:1000; Cell signaling 2578), Histone H3 Antibody (1:1000; Cell signaling 9715), Histone H4 (1:1000; Cell signaling 2592). (C) 2D Western Blot. Red ponceau Staining of membranes and image master analysis. For 2D Western blot analysis, equal amounts of histone extracts were resolved by 2D TAU/SDS gel. To minimize gel to gel variation and ensure a reliable comparison among analyzed samples second dimension for each sample was run on Mini-PROTEAN® TGX™ Precast Gels, IPG Well (15%). Resulting gel were transferred to nitrocellulose membranes with a Trans-blot turbo system (Biorad) using Trans-Blot® Turbo™ Mini Nitrocellulose Transfer Packs. To ensure equal protein loading, membranes were incubated with red ponceau solution (P7170 Sigma-Aldrich). Images were acquired using Image scanner II (GE Helthcare). Membrane image were visualized using image master 2D platinum. 3D visualization tool testify the loading of equal amount for each Histone extract (panel D).

Sequence: KASGPPVSELITK, K1-Dimethyl (28.03130 Da)

Charge: +2, Monoisotopic m/z: 677.90155 Da (+0.86 mmu/+1.26 ppm), MH⁺: 1354.79582 Da, RT: 19.59 min,

Identified with: Sequest HT (v1.3); XCorr:3.93, Ions matched by search engine: 0/0

Fragment match tolerance used for search: 0.02 Da



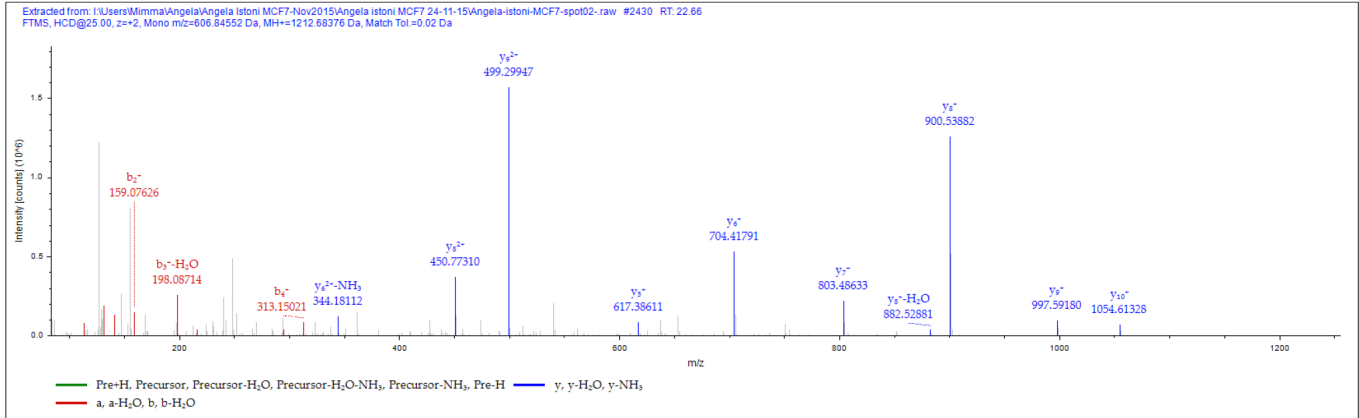
#1	a ⁺	a ²⁺	b ⁺	b ²⁺	Seq.	y ⁺	y ²⁺	#2
1	12.913.863	6.507.295	15.713.355	7.907.041	K-Dimethyl			13
2	20.017.575	10.059.151	22.817.067	11.458.897	A	119.866.784	59.983.756	12
3	28.720.778	14.410.753	31.520.270	15.810.499	S	112.763.072	56.431.900	11
4	34.422.925	17.261.826	37.222.417	18.661.572	G	104.059.869	52.080.298	10
5	44.128.202	22.114.465	46.927.694	23.514.211	P	98.357.722	49.229.225	9
6	53.833.479	26.967.103	56.632.971	28.366.849	P	88.652.445	44.376.586	8
7	63.740.321	31.920.524	66.539.813	33.320.270	V	78.947.168	39.523.948	7
8	72.443.524	36.272.126	75.243.016	37.671.872	S	69.040.326	34.570.527	6
9	85.347.784	42.724.256	88.147.276	44.124.002	E	60.337.123	30.218.925	5
10	96.656.191	48.378.459	99.455.683	49.778.205	L	47.432.863	23.766.795	4
11	107.964.598	54.032.663	110.764.090	55.432.409	I	36.124.456	18.112.592	3
12	118.069.366	59.085.047	120.868.858	60.484.793	T	24.816.049	12.458.388	2
13					K	14.711.281	7.406.004	1

Sequence: ASGPPVSELITK, K12-Methyl (14.01565 Da)

Charge: +2, Monoisotopic m/z: 606.84552 Da (+0.14 mmu/+0.22 ppm), MH+: 1212.68376 Da, RT: 22.66 min,

Identified with: Sequest HT (v1.3); XCorr:2.25, Ions matched by search engine: 0/0

Fragment match tolerance used for search: 0.02 Da



#1	a ⁺	a ²⁺	b ⁺	b ²⁺	Seq.	y ⁺	y ²⁺	#2
1	4.404.948	2.252.838	7.204.440	3.652.584	A			12
2	13.108.151	6.604.439	15.907.643	8.004.185	S	114.164.637	57.132.682	11
3	18.810.298	9.455.513	21.609.790	10.855.259	G	105.461.434	52.781.081	10
4	28.515.575	14.308.151	31.315.067	15.707.897	P	99.759.287	49.930.007	9
5	38.220.852	19.160.790	41.020.344	20.560.536	P	90.054.010	45.077.369	8
6	48.127.694	24.114.211	50.927.186	25.513.957	V	80.348.733	40.224.730	7
7	56.830.897	28.465.812	59.630.389	29.865.558	S	70.441.891	35.271.309	6
8	69.735.157	34.917.942	72.534.649	36.317.688	E	61.738.688	30.919.708	5
9	81.043.564	40.572.146	83.843.056	41.971.892	L	48.834.428	24.467.578	4
10	92.351.971	46.226.349	95.151.463	47.626.095	I	37.526.021	18.813.374	3
11	102.456.739	51.278.733	105.256.231	52.678.479	T	26.217.614	13.159.171	2
12					K-Methyl	16.112.846	8.106.787	1

ALAAAGYDVEK_{Methyl}

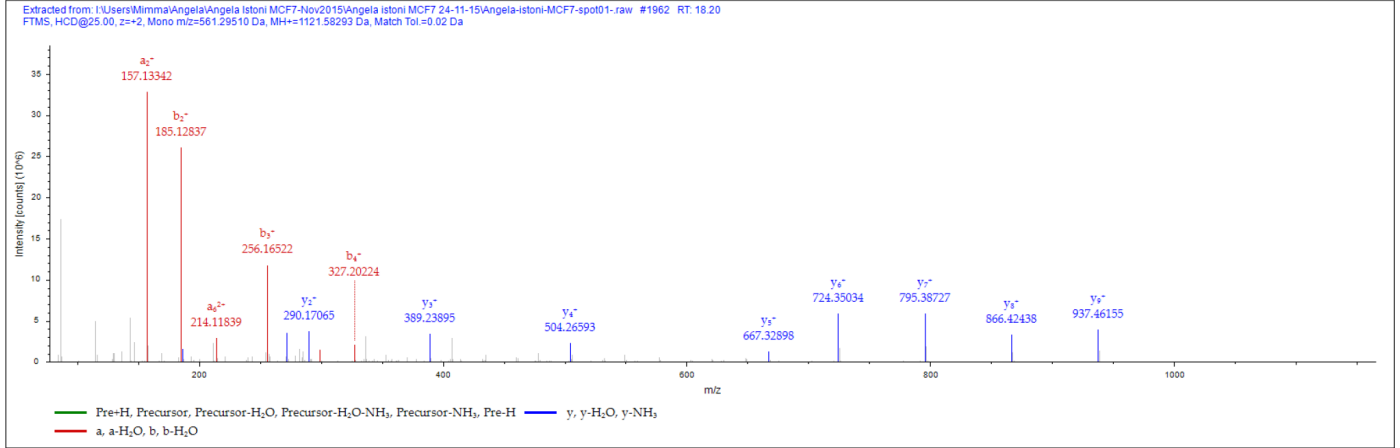
H1.2K74 – H1.3K75

Sequence: ALAAAGYDVEK, K11-Methyl (14.01565 Da)

Charge: +2, Monoisotopic m/z: 561.29510 Da (-0.42 mmu/-0.75 ppm), MH+: 1121.58293 Da, RT: 18.20 min,

Identified with: Sequest HT (v1.3); XCorr:3.13, Ions matched by search engine: 0/0

Fragment match tolerance used for search: 0.02 Da



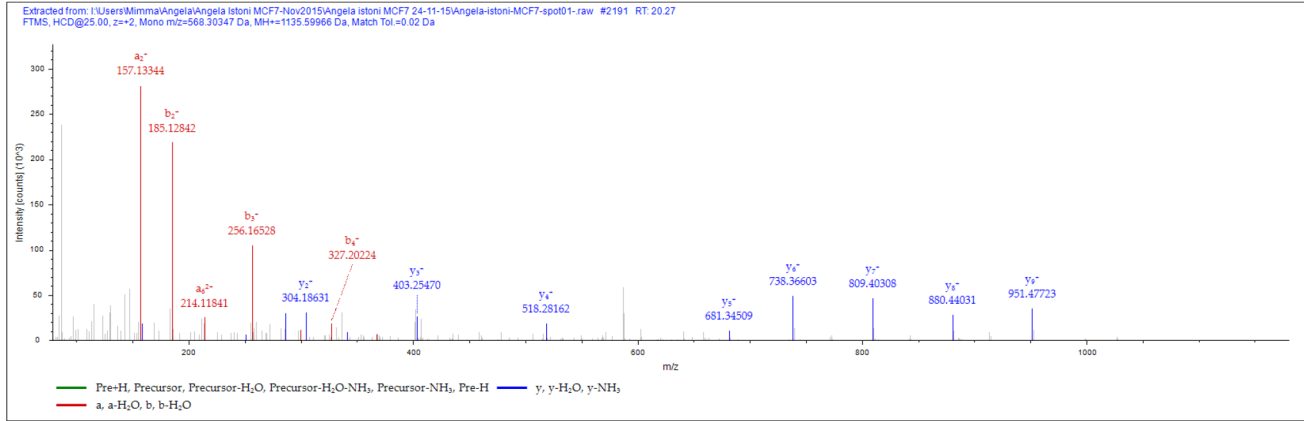
#1	a ⁺	a ²⁺	b ⁺	b ²⁺	Seq.	y ⁺	y ²⁺	#2
1	4.404.948	2.252.838	7.204.440	3.652.584	A			11
2	15.713.355	7.907.041	18.512.847	9.306.787	L	105.054.665	52.577.696	10
3	22.817.067	11.458.897	25.616.559	12.858.643	A	93.746.258	46.923.493	9
4	29.920.779	15.010.753	32.720.271	16.410.499	A	86.642.546	43.371.637	8
5	37.024.491	18.562.609	39.823.983	19.962.355	A	79.538.834	39.819.781	7
6	42.726.638	21.413.683	45.526.130	22.813.429	G	72.435.122	36.267.925	6
7	59.032.970	29.566.849	61.832.462	30.966.595	Y	66.732.975	33.416.851	5
8	70.535.665	35.318.196	73.335.157	36.717.942	D	50.426.643	25.263.685	4
9	80.442.507	40.271.617	83.241.999	41.671.363	V	38.923.948	19.512.338	3
10	93.346.767	46.723.747	96.146.259	48.123.493	E	29.017.106	14.558.917	2
11					K-Methyl	16.112.846	8.106.787	1

Sequence: ALAAAGYDVEK, K11-Dimethyl (28.03130 Da)

Charge: +2, Monoisotopic m/z: 568.30347 Da (+0.12 mmu/+0.21 ppm), MH⁺: 1135.59966 Da, RT: 20.27 min,

Identified with: Sequest HT (v1.3); XCorr:2.87, Ions matched by search engine: 0/0

Fragment match tolerance used for search: 0.02 Da

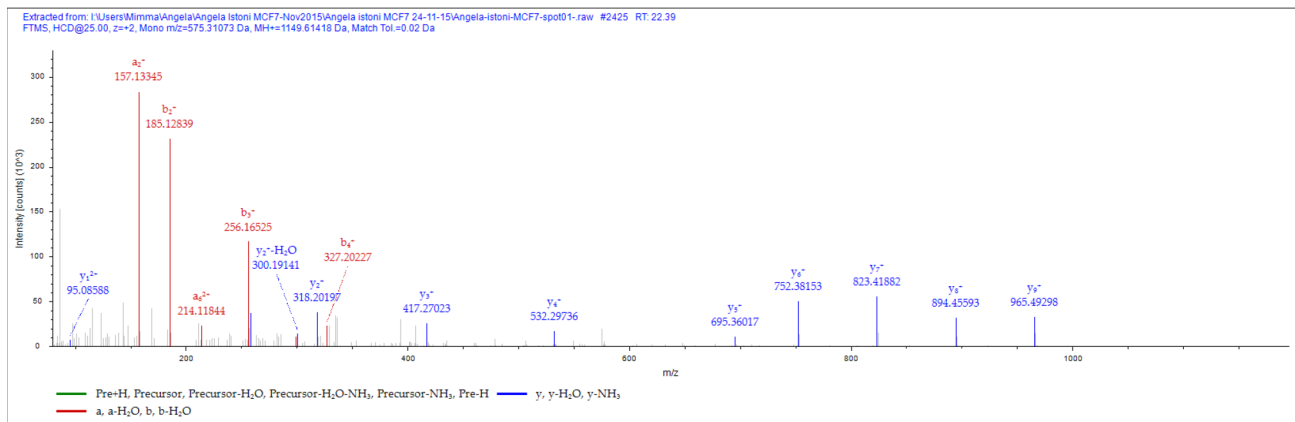


#1	a ⁺	a ²⁺	b ⁺	b ²⁺	Seq.	y ⁺	y ²⁺	#2
1	4.404.948	2.252.838	7.204.440	3.652.584	A			11
2	15.713.355	7.907.041	18.512.847	9.306.787	L	106.456.230	53.278.479	10
3	22.817.067	11.458.897	25.616.559	12.858.643	A	95.147.823	47.624.275	9
4	29.920.779	15.010.753	32.720.271	16.410.499	A	88.044.111	44.072.419	8
5	37.024.491	18.562.609	39.823.983	19.962.355	A	80.940.399	40.520.563	7
6	42.726.638	21.413.683	45.526.130	22.813.429	G	73.836.687	36.968.707	6
7	59.032.970	29.566.849	61.832.462	30.966.595	Y	68.134.540	34.117.634	5
8	70.535.665	35.318.196	73.335.157	36.717.942	D	51.828.208	25.964.468	4
9	80.442.507	40.271.617	83.241.999	41.671.363	V	40.325.513	20.213.120	3
10	93.346.767	46.723.747	96.146.259	48.123.493	E	30.418.671	15.259.699	2
11					K-Dimethyl	17.514.411	8.807.569	1

ALAAAGYDVEK_{Trimethyl}

H1.3K75

Sequence: ALAAAGYDVEK, K11-Trimethyl (42.04695 Da)
 Charge: +2, Monoisotopic m/z: 575.31073 Da (-0.44 mmu/-0.77 ppm), MH+: 1149.61418 Da, RT: 22.39 min,
 Identified with: Sequest HT (v1.3); XCorr:2.95, Ions matched by search engine: 0/0
 Fragment match tolerance used for search: 0.02 Da



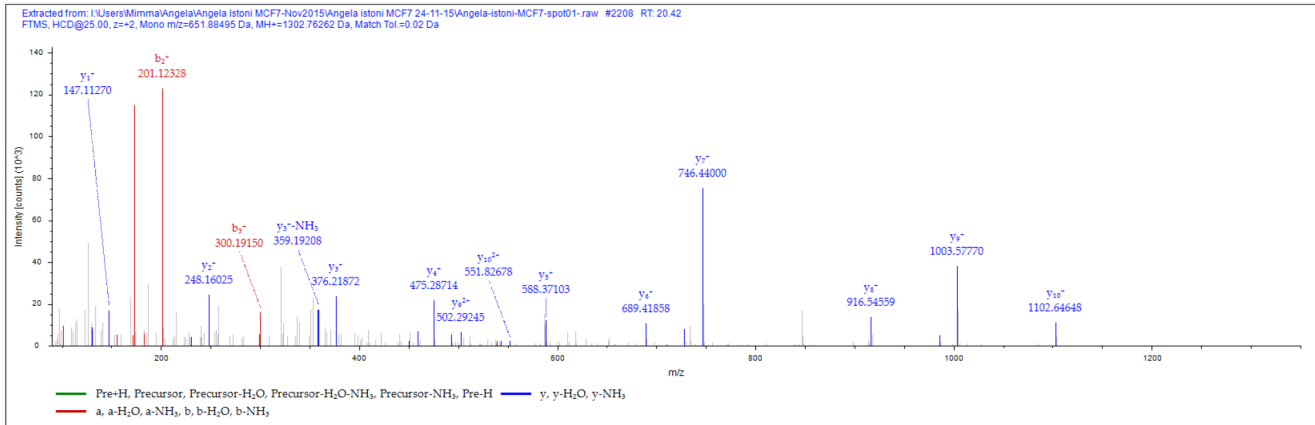
#1	a*	a2*	b*	b2*	Seq.	y*	y2*	#2
1	4.404.948	2.252.838	7.204.440	3.652.584	A			11
2	15.713.355	7.907.041	18.512.847	9.306.787	L	107.857.795	53.979.261	10
3	22.817.067	11.458.897	25.616.559	12.858.643	A	96.549.388	48.325.058	9
4	29.920.779	15.010.753	32.720.271	16.410.499	A	89.445.676	44.773.202	8
5	37.024.491	18.562.609	39.823.983	19.962.355	A	82.341.964	41.221.346	7
6	42.726.638	21.413.683	45.526.130	22.813.429	G	75.238.252	37.669.490	6
7	59.032.970	29.566.849	61.832.462	30.966.595	Y	69.536.105	34.818.416	5
8	70.535.665	35.318.196	73.335.157	36.717.942	D	53.229.773	26.665.250	4
9	80.442.507	40.271.617	83.241.999	41.671.363	V	41.727.078	20.913.903	3
10	93.346.767	46.723.747	96.146.259	48.123.493	E	31.820.236	15.960.482	2
11					K-Trimethyl	18.915.976	9.508.352	1

Sequence: SLVSKGTLVQTK, K5-Acetyl (42.01057 Da)

Charge: +2, Monoisotopic m/z: 651.88495 Da (-0.09 mmu/-0.13 ppm), MH+: 1302.76262 Da, RT: 20.42 min,

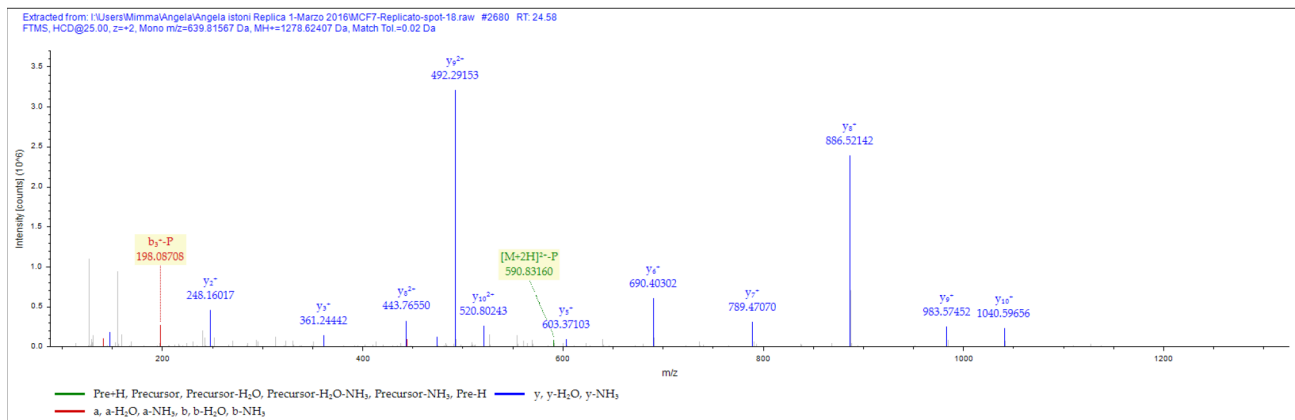
Identified with: Sequest HT (v1.3); XCorr:3.03, Ions matched by search engine: 0/0

Fragment match tolerance used for search: 0.02 Da



#1	a*	a2*	b*	b2*	Seq.	y*	y2*	#2
1	6.004.439	3.052.583	8.803.931	4.452.329	S			12
2	17.312.846	8.706.787	20.112.338	10.106.533	L	121.573.077	60.836.902	11
3	27.219.688	13.660.208	30.019.180	15.059.954	V	110.264.670	55.182.699	10
4	35.922.891	18.011.809	38.722.383	19.411.555	S	100.357.828	50.229.278	9
5	52.933.445	26.517.086	55.732.936	27.916.832	K-Acetyl	91.654.625	45.877.676	8
6	58.635.592	29.368.160	61.435.083	30.767.905	G	74.644.071	37.372.399	7
7	68.740.360	34.420.544	71.539.851	35.820.289	T	68.941.924	34.521.326	6
8	80.048.767	40.074.747	82.848.258	41.474.493	L	58.837.156	29.468.942	5
9	89.955.609	45.028.168	92.755.100	46.427.914	V	47.528.749	23.814.738	4
10	102.761.467	51.431.097	105.560.958	52.830.843	Q	37.621.907	18.861.317	3
11	112.866.235	56.483.481	115.665.726	57.883.227	T	24.816.049	12.458.388	2
12					K	14.711.281	7.406.004	1

Sequence: ASGPPVSELITK, S2-Phospho (79.96633 Da)
 Charge: +2, Monoisotopic m/z: 639.81567 Da (-5.05 mmu/-7.9 ppm), MH+: 1278.62407 Da, RT: 24.58 min,
 Identified with: Sequest HT (v1.3); XCorr:2.86, Ions matched by search engine: 0/0
 Fragment match tolerance used for search: 0.02 Da



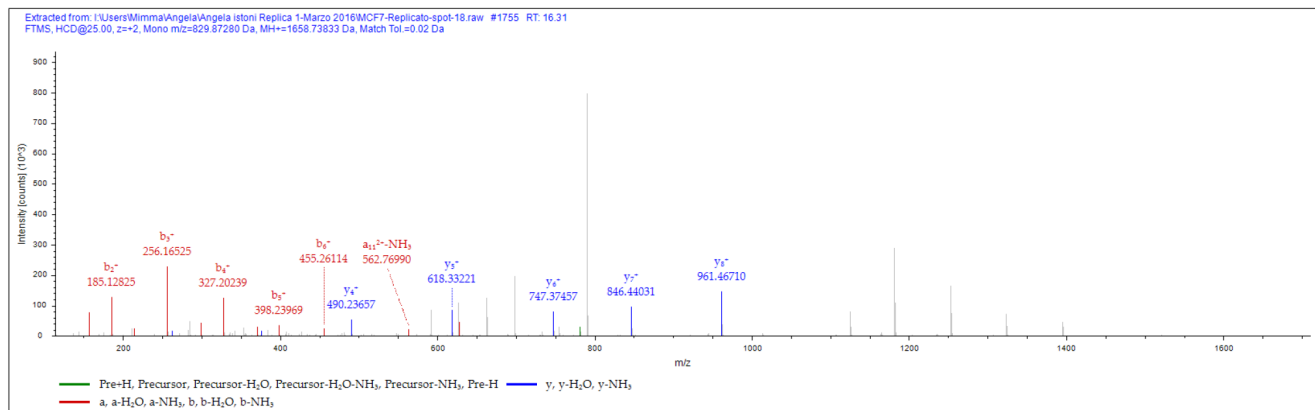
#1	a ⁺	a ²⁺	b ⁺	b ²⁺	Seq.	y ⁺	y ²⁺	#2
1	4.404.948	2.252.838	7.204.440	3.652.584	A			12
2	21.104.784	10.602.756	23.904.276	12.002.502	S-Phospho	120.759.705	60.430.216	11
3	26.806.931	13.453.829	29.606.423	14.853.575	G	104.059.869	52.080.298	10
4	36.512.208	18.306.468	39.311.700	19.706.214	P	98.357.722	49.229.225	9
5	46.217.485	23.159.106	49.016.977	24.558.852	P	88.652.445	44.376.586	8
6	56.124.327	28.112.527	58.923.819	29.512.273	V	78.947.168	39.523.948	7
7	64.827.530	32.464.129	67.627.022	33.863.875	S	69.040.326	34.570.527	6
8	77.731.790	38.916.259	80.531.282	40.316.005	E	60.337.123	30.218.925	5
9	89.040.197	44.570.462	91.839.689	45.970.208	L	47.432.863	23.766.795	4
10	100.348.604	50.224.666	103.148.096	51.624.412	I	36.124.456	18.112.592	3
11	110.453.372	55.277.050	113.252.864	56.676.796	T	24.816.049	12.458.388	2
12					K	14.711.281	7.406.004	1

Sequence: ALAAAGYDVEKNNSR, Y7-Phospho (79.96633 Da)

Charge: +2, Monoisotopic m/z: 829.87280 Da (-7.57 mmu/-9.12 ppm), MH+: 1658.73833 Da, RT: 16.31 min,

Identified with: Sequest HT (v1.3); XCorr:2.90, Ions matched by search engine: 0/0

Fragment match tolerance used for search: 0.02 Da



#1	a ⁺	a ²⁺	b ⁺	b ²⁺	Seq.	y ⁺	y ²⁺	#2
1	44.04948	22.52838	72.04440	36.52584	A			15
2	157.13355	79.07041	185.12847	93.06787	L	1587.71634	794.36181	14
3	228.17067	114.58897	256.16559	128.58643	A	1474.63227	737.81977	13
4	299.20779	150.10753	327.20271	164.10499	A	1403.59515	702.30121	12
5	370.24491	185.62609	398.23983	199.62355	A	1332.55803	666.78265	11
6	427.26638	214.13683	455.26130	228.13429	G	1261.52091	631.26409	10
7	670.29603	335.65165	698.29095	349.64911	Y-Phospho	1204.49944	602.75336	9
8	785.32298	393.16513	813.31790	407.16259	D	961.46979	481.23853	8
9	884.39140	442.69934	912.38632	456.69680	V	846.44284	423.72506	7
10	1013.43400	507.22064	1041.42892	521.21810	E	747.37442	374.19085	6
11	1141.52897	571.26812	1169.52389	585.26558	K	618.33182	309.66955	5
12	1255.57190	628.28959	1283.56682	642.28705	N	490.23685	245.62206	4
13	1369.61483	685.31105	1397.60975	699.30851	N	376.19392	188.60060	3
14	1456.64686	728.82707	1484.64178	742.82453	S	262.15099	131.57913	2
15					R	175.11896	88.06312	1

Supplementary Figure 3. Fragmentation MS/MS spectra of the modified peptide carrying identified PTMs. MS/MS data are referred to all analyzed histones. Data were analyzed by Proteome Discoverer 1.4 software. MS/MS data were searched on the Human UniProt database. For each PTM we reported: Sequence, type of modification, Charge, m/z, and RT.